Check for updates

ADVANCED FUNCTIONAL MATERIALS
www.afm-journal.de

Recent Advances in Enzyme-based Biofuel Cells Using Glucose Fuel: Achieving High Power Output and Enhanced Operational Stability

Junha Pak, Woojae Chang, Cheong Hoon Kwon, and Jinhan Cho**

An enzyme-based biofuel cell (EBFC) is widely regarded as one of the most efficient power sources for bio-friendly and implantable medical devices, capable of converting electrochemical reactions into electrical currents under physiological conditions. However, despite its potential, the practical and commercial use of EBFCs is limited by their low power output and operational instability. Therefore, significant research efforts have focused on increasing power output and stability by improving electron transfer between enzymes and host electrodes and developing efficient enzyme immobilization techniques. However, most EBFCs produced by current methods still deliver unsatisfactory performance. A promising approach to address these challenges is the use of conductive linkers that promote favorable interfacial interactions between adjacent enzymes and between enzymes and host electrodes. These linkers can facilitate electron transfer and ensure robust enzyme immobilization. In addition, designing the host electrode with a 3D structure and a large surface area can further improve the areal energy performance. This perspective reviews the working principles, types, and electron transfer mechanisms of EBFC electrodes and explores how conductive linkers and 3D host electrodes can enhance the performance of EBFC electrodes. Finally, recent advances in integrating EBFCs into biomedical devices are described.

1. Introduction

The rapid expansion of portable and medical electronic devices, including micro-scale and implantable systems, has led to an increasing demand for renewable and sustainable energy sources. To address this need, enzyme-based biofuel cells (EBFCs), which can generate electricity from biofuels such as glucose and oxygen using enzymes found in the physiological fluids of living organisms, have emerged as a promising alternative.[1–15] In particular, the environmentally friendly nature of EBFCs makes them an attractive power source for implantable medical devices.

Typically, EBFCs using glucose fuel are based on a two-electrode system consisting of an anode and a cathode. At the anode, enzymes such as glucose oxidase (GOx) and glucose dehydrogenase (GDH) play crucial roles in oxidizing biofuels.[16,17] Unlike GOx, GDH offers the advantage of not producing hydrogen peroxide (H_2O_2) during glucose oxidation, a byproduct that can cause electrode degradation. Additionally, GDH exhibits optimal activity near pH 7, which closely aligns with physiological conditions, making it particularly suitable for EBFC applications.[18] On the other hand, GOx is widely recognized as a promising enzyme due to its high specificity for glucose and rapid kinetics, both of which enhance the power density of the EBFCs.[19] Ultimately, these enzymes catalyze the oxidation of glucose to gluconolactone, generating electrons that can be harnessed for energy production in EBFCs. At the cathode, enzyme catalysts such as laccase (Lac), bilirubin oxidase (BOD), and tyrosinase are utilized to drive the oxygen reduction reaction (ORR). In addition, inorganic catalysts such as gold (Au), platinum (Pt), palladium (Pd), cobalt (Co), and ruthenium (Ru) have also been employed.[20–22] These catalysts induce the ORR by

J. Pak, W. Chang, J. Cho
Department of Chemical and Biological Engineering
Korea University
145 Anam-ro, Seongbuk-gu, Seoul 02841, Republic of Korea
E-mail: jinhan71@korea.ac.kr

C. H. Kwon
Department of Energy Resources and Chemical Engineering
Kangwon National University
346 Jungang-ro, Samcheok 25913, Republic of Korea
E-mail: chkwon2@kangwon.ac.kr

J. Cho
KU-KIST Graduate School of Converging Science and Technology
Korea University
145 Anam-ro, Seongbuk-gu, Seoul 02841, Republic of Korea

J. Cho
Soft Hybrid Materials Research Center
Advanced Materials Research Division
Korea Institute of Science and Technology (KIST)
5 Hwarang-ro 14-gil, Seongbuk-gu, Seoul 02792, Republic of Korea

The ORCID identification number(s) for the author(s) of this article can be found under https://doi.org/10.1002/adfm.202415933

© 2024 The Author(s). Advanced Functional Materials published by Wiley-VCH GmbH. This is an open access article under the terms of the Creative Commons Attribution-NonCommercial License, which permits use, distribution and reproduction in any medium, provided the original work is properly cited and is not used for commercial purposes.

DOI: 10.1002/adfm.202415933

facilitating the reduction of oxygen to water through electron acceptance.

Despite the availability of various electrocatalysts for EBFC electrodes, EBFCs still face significant challenges in terms of low power output and poor operational stability, particularly when compared to other power sources such as conventional fuel cells, supercapacitors, and batteries. These limitations severely hinder the practical applications of EBFCs.[7,23–28] To address these critical issues, substantial research have been dedicated to enhancing the power performance and operational stability of EBFCs beyond the levels reported to date.[29–33] These efforts have primarily focused on optimizing electron transfer between enzymes and host electrodes, as well as between adjacent enzymes, and improving the effective immobilization of the enzyme on the host electrode.[34–36] However, for EBFCs, the poor electrical conductivity of electrocatalytic enzymes, coupled with the lack of suitable anode alternatives, remains a major obstacle to enhancing the overall performance of EBFCs for use in implantable medical devices.

One approach to enhance electron transfer between the host electrode and enzyme is to incorporate redox mediators with long space arms containing electron hopping sites into the enzyme material.[15,37–40] For example, GOx, an enzyme widely used in EBFC anodes, has an active site (flavin adenine dinucleotide, FAD) buried ≈7–15 Å below the insulating protein surface.[41] This burial significantly restricts the electron transfer between the enzyme and the host electrode, as well as between adjacent enzymes, thereby reducing the enzyme activity relative to its loading amount on the host electrode surface. This low enzyme activity directly contributes to the low areal power density of EBFCs.[42–44] Therefore, the incorporation of redox mediators with active site-containing long space arms, such as osmium (Os)-based polymeric mediators, can significantly increase the possibility of external electrons reaching the deeply buried FAD center within the GOx in the electrolyte solution.[36,37] These redox mediators can also increase enzyme activity by facilitating electron transfer, allowing higher enzyme loading.[45–47] Consequently, electron transfer via these redox mediators, known as mediated electron transfer (MET), is the preferred electron transfer mechanism in EBFCs designed for high-power generation. Several research groups reported MET-EBFCs with remarkably high areal power densities in the range of 1 to 2 mW cm^{-2} about 5–10 years ago.[48,49] However, since then, there has been little notable progress in terms of power output.

Most of the MET-based electrodes reported to date have been mainly fabricated by mechanically mixed slurries of enzymes, mediators, and cross–linking agents on the host electrode.[49–52] This slurry coating method often results in the inclusion of excess enzymes unbound to the mediators, the non-uniform mixing of enzymes and mediators, and the presence of insulating cross–linkers, all of which impede electron transfer within the enzyme electrode, even with MET. As a result, achieving higher power performance and operational stability for EBFCs has become challenging. Although researchers have aimed to develop more unique redox mediators to facilitate electron hopping pathways to the enzymes, these efforts face additional obstacles, including complicated synthesis, toxicity, leaching, and instability of these redox mediators, and a reduction of the open-circuit voltage (OCV) to below 0.8 V, all of which further complicate the pursuit of high-performance EBFCs.[48,49,53,54]

Another research effort has focused on the development of high-performance EBFCs based on direct electron transfer (DET-EBFCs) without the use of redox mediators. However, achieving high-performance DET-EBFCs without the aid of redox mediators and conductive components is fundamentally challenging due to the poor electron transfer between enzymes and host electrodes, as well as between adjacent enzymes. Due to these critical issues, DET-EBFCs typically exhibit significantly low power efficiencies, ranging from a few to hundreds of μW cm^{-2}, which has severely limited their use in various biomedical industries, including as pacemakers and cardioverter defibrillators.[55,56] To overcome these issues, various conductive materials (i.e., carbon nanotubes (CNTs), metal nanoparticles (NPs), and conducting polymers) were incorporated into enzyme layers to facilitate the electron relay effect.[57–63] This electron relay has enhanced the power performance of DET-EBFCs. For example, Kang and colleagues reported that by depositing the GOx/conductive indium tin oxide (ITO) NP multilayers on a host electrode through consecutive interfacial interactions between GOx and ITO NPs as the anode and using a Pt-sputtered host electrode as the cathode, the power output of the resulting DET-EBFC was increased to 1.4 mW cm^{-2} at 10 mmol L^{-1} glucose concentration.[64] Furthermore, they demonstrated that by introducing additional structural modifications to the host electrode, the power performance of the DET-EBFC could be further increased up to 2.0 mW cm^{-2} at the same glucose concentration.

Another important factor affecting the power performance and operational stability of EBFCs is enzyme immobilization.[65,66] As mentioned earlier, in the case of GOx, to facilitate effective electron transfer, the active sites (FAD) buried below the insulating protein shell require a minimum distance from the surface of the host electrode and adjacent enzymes to facilitate effective electron transfer.[67–69] This minimum distance can be achieved by favorable interfacial interactions (i.e., electrostatic interaction, hydrogen bonding, and/or covalent bonding interactions) between two different components, entrapment, or precipitation with cross–linking. Furthermore, the formation of the favorable interactions effectively prevents the detachment of active components from EBFC electrodes (specifically, the detachment of the enzymes and/or conductive components from DET-EBFC electrode or the detachment of the enzymes, conductive components, and/or redox mediators from MET-EBFC electrode), which can significantly contribute to the improvement of the operational stability of EBFCs. Therefore, if all the active components can be robustly bridged with each other without inactive components such as binders, and simultaneously their overall thickness can be controlled for optimal electron transfer, such a structural and interfacial electrode design can provide a simple and effective way to develop the high-performance EBFC electrodes. In particular, owing to the presence of amino acid groups in enzymes that allow hydrogen bonding and electrostatic interactions, a layer-by-layer (LbL) assembly technique, which is based on complementary interfacial interactions between adjacent components, can be effectively utilized to fabricate robust enzyme films with controlled thin thickness on various host electrodes. This approach allows the integration of enzymes with other active components, such

© 2024 The Author(s). Advanced Functional Materials published by Wiley-VCH GmbH

16163028, 2025, 16, Downloaded from https://advanced.onlinelibrary.wiley.com/doi/10.1002/adfm.202415933 by Korea University Library, Wiley Online Library on [20/09/2026]. See the Terms and Conditions (https://onlinelibrary.wiley.com/terms-and-conditions) on Wiley Online Library for rules of use; OA articles are governed by the applicable Creative Commons License

as conductive components and/or redox mediators, resulting in enhanced power performance and operational stability.

Furthermore, it is important to highlight that the LbL assembly based on solution dipping is highly effective for the deposition of various functional components (i.e., enzymes, conductive components, and/or redox mediators) on highly porous 3D host electrodes with diverse form factors. This approach can significantly increase the loading amounts of functional components per unit area, enabling efficient electron transfer throughout the entire regions of 3D host electrodes, from the exterior to the interior. This improvement directly contributes to the enhanced power output of EBFCs. Therefore, we believe that the effective integration of interfacial interaction-mediated LbL assembly with 3D host electrodes can play a pivotal role in boosting the power output and operational stability of not only glucose-based EBFCs but also other types of EBFCs. To our knowledge, no previous reviews or perspective papers on EBFCs have addressed this combined approach.

In this perspective, we discuss recent approaches and advances to achieve high-power performance and stable operation in glucose-based EBFCs by optimizing electron transfer within the electrodes. In addition, we demonstrate that an interfacial assembly approach based on complementary interactions between adjacent electrode components can significantly contribute to electron transfer and enzyme immobilization simultaneously. First, we introduce the energy conversion mechanism occurring at the EBFC anode and cathode, the various approaches for enzyme immobilization, and the role of each electrode component in the EBFC electrode. Based on the role of these electrode components, we will show various approaches to develop high-performance EBFC electrodes, particularly DET-EBFC electrodes using the electron relay effect. Additionally, we will elucidate how a robust interfacial interaction-induced LbL assembly approach of electrode components, a 3D host electrode with a large surface area, and a structural design of overall electrodes can enhance the electron transfer, power output, and operational stability of DET-EBFCs. Furthermore, we review recent research trends in EBFCs for biomedical applications. Finally, we briefly outline the improvements in interfacial assembly techniques to advance the development of next-generation EBFC devices with enhanced performance.

2. Energy Conversion of Glucose-based EBFCs

2.1. Working Principle of Glucose-based EBFCs

Glucose-based EBFCs, which consist of an anode coated with enzymes (mainly GOx), and a cathode coated with ORR catalysts, including biocompatible metal catalysts (Au NPs or Pt NPs), BOD, or Lac, perform electrochemical reactions in a phosphate buffered saline (PBS) solution containing oxygen and glucose fuel as follows:

$$\text{Anode}: \quad 2\ \text{glucose} \rightarrow 2\ \text{gluconolactone} + 4H^+ + 4e^- \tag{1}$$

$$\text{Cathode}: \quad O_2 + 4H^+ + 4e^- \rightarrow 2H_2O \tag{2}$$

$$\text{Complete cell}: \quad 2\ \text{glucose} + O_2 \rightarrow 2\ \text{gluconolactone} + 2H_2O \tag{3}$$

First, the glucose fuel undergoes an enzyme-catalyzed oxidation at the anode, converting it to gluconolactone and producing electrons that transverse through an external circuit to reach the cathode. At the cathode, oxygen is converted to water by ORR catalysts, such as BOD, Au NPs, or Pt NPs, resulting in a net electric current flow.[5] Equations 1 and 2 show the corresponding electron generation and ORR using enzymatic catalysts and ORR catalysts at the anode and cathode, respectively.[70] The overall reaction of the complete BFCs follows Equation 3. Consequently, if the electron transfer from enzymes to the host electrode at the anode is impeded by high resistances (due to the increased separation distance between the active sites of the enzymes and the host electrode as well as the electrical conductivity of the host electrode) and/or the ORR efficiency at the cathode is diminished by inefficient catalysts and/or the low electrical conductivity of the host electrode, the overall power output of the complete cell device will be significantly reduced.[6,71]

To enhance the efficiency of the ORR at the cathode, a variety of inorganic catalysts (i.e., Au, Pt, Pd, Co, and Ru), are commonly utilized. For example, Ru and Pt facilitate the ORR by adsorbing oxygen onto their surfaces, where oxygen molecules accept electrons and form hydroxide ions (OH^-). These OH^- then react with additional hydrogen ions (H^+) to produce water. On the other hand, Pd catalyzes the production of H_2O_2 by adsorbing oxygen and accepting electrons. The H_2O_2 then subsequently undergoes further reduction in the ORR pathway, ultimately leading to water production in the presence of additional electrons and H^+. In addition to inorganic catalysts, enzyme catalysts, such as Lac, BOD, and tyrosinase, are also used for their ability to catalyze oxygen reduction.[20–22] These enzymes possess active sites that bind to substrates, inducing substrate oxidation and the release of electrons. The released electrons are transferred through the enzyme's electron transport chain, where they interact with oxygen molecules, reducing them to OH^- or water, thereby contributing to water production along with the oxidized substrate. The careful selection and effective use of both inorganic or enzymatic catalysts at the cathode are critical to optimizing ORR efficiency and, consequently, the overall performance of EBFCs.

However, a major challenge in developing high-performance glucose-based EBFCs lies in improving the efficiency of electron transfer between the enzymes and the host electrode at the anode, which remains a key area for further research and innovation.[72] The operating mechanisms at the anode, with different approaches to improve the efficiency of electron transfer at the anode, are described in more detail in Sections 2.2 and 2.3.

2.2. Electron Transfer in Glucose-based EBFCs

2.2.1. Glucose-based MET-EBFCs

In the MET-EBFCs, a variety of redox components, along with certain redox proteins, serve as mediators capable of shuttling electrons between the host electrode and the enzyme.[57,73] Essentially, the redox mediators, including pyridine or pyridine derivatives, ferrocene, Meldola's blue, and Os redox polymers (e.g., $Os(2,2'\text{-bipyridine})_2(\text{polyvinylimidazole})_{10}Cl)^{+/2+}$, shortly referred to as $Os(bpy)_2PVI$), accept electrons generated from the fuel. These electrons are then transferred to the cathode, where

© 2024 The Author(s). Advanced Functional Materials published by Wiley-VCH GmbH

16163028, 2025, 16, Downloaded from https://advanced.onlinelibrary.wiley.com/doi/10.1002/adfm.202415933 by Korea University Library, Wiley Online Library on [20/09/2026]. See the Terms and Conditions (https://onlinelibrary.wiley.com/terms-and-conditions) on Wiley Online Library for rules of use; OA articles are governed by the applicable Creative Commons License

they combine with oxygen to generate electricity.[2,74–76] Generally, these mediators are mixed with enzymes and cross–linking agents and then deposited onto the host electrode through the slurry coating.

In particular, among the various redox mediators, the Os ion-based redox polymers have been considered as one of the most promising mediator candidates for high-performance MET-EBFCs. This is due to the efficient electron transfer facilitated by Os ion centers with elongated spacer arms, which significantly enhance the electron transfer rates between the electrode surface and redox active species.[77–79] This high electron transfer directly translates into improved electrochemical performance, thereby enhancing EBFC efficiency. Furthermore, another notable advantage of Os redox polymers is that their properties can be tailored to specific medical applications. This customization is achieved by adjusting factors such as polymer composition, molecular weight, and redox potential, thereby optimizing several key energy performance indices of EBFC electrodes, including electron transfer kinetics, charge storage capacity, electrochemical stability, and operating efficiency.[70]

Based on these unique electrochemical properties, various types of Os redox polymers have been synthesized and applied to MET-EBFCs. For instance, Gao et al. reported CNT-based MET-EBFCs composed of PVP-[Os(*N*,*N*′-alkylanated-2,2′bi-imidazole)$_3$]$^{2+/3}$-mediated GOx anode and poly(acryl amide) (PAA)-PVI-[Os(4,4′-dichloro-2,2′-bipyridine)$_2$Cl]$^{+/2+}$-mediated BOD cathode (**Figure 1a**).[80] The incorporation of CNTs significantly improved the performance due to their high porosity and electrical conductivity. Field-emission scanning electron microscopy (FE-SEM) images showed distinct structural differences between non-porous carbon fiber and porous CNT microwires (Figure 1b,c). This structural advantage was reflected in the superior electrochemical performance of the CNT-based electrode, as demonstrated by cyclic voltammetry (CV) comparisons (Figure 1d,e). The CNT-based MET-EBFC achieved a maximum power output of 740 μW cm^{-2} and an OCV of 0.83 V, outperforming the carbon-based MET-EBFC, which produced 180 μW cm^{-2} and an OCV of 0.73 V under the same condition, at the glucose concentration of 15 mmol L^{-1} in PBS (Figure 1f).

Additionally, CNT fiber-based bioelectrocatalysts are more stable than their carbon fiber-based counterparts (Figure 1g). While carbon fiber poised at +0.3 V (versus Ag/AgCl) and at 37 °C loses 80% of its current density in 8 h, CNT fiber loses only 18% of its initial current density under the same conditions. This result indicates that CNT fibers enhance the bioelectrocatalyst by forming a strong three-dimensional composite. Moreover, Xiao et al. reported the MET-EBFCs based on the Os redox polymer (i.e., Os(bpy)$_2$PVI)-mediated GOx anode and the Os(bpy)$_2$PVI-mediated BOD cathode, which can be used as a self-powered drug-release system in vivo.[81] In this case, when the MET-EBFC was discharged in the presence of glucose and oxygen, the drug components incorporated in the conductive polymer layer onto the cathode were rapidly released.

Yuasa's group introduced a novel approach to MET-EBFCs by developing a FAD-dependent GDH-based biofuel cell that utilizes poly(glycidyl methacrylate) (poly(GMA))- grafted-MgO templated porous carbon (MgOC) as the substrate, with aminoferrocene (AmFc) serving as the redox mediator.[82] The poly(GMA) provided glycidyl groups for covalent bonding with the amino groups of AmFc and FAD-GDH. This bonding reduced the distance between the mediator and enzyme, thereby enhancing the overall performance of the glucose-based EBFC. The device demonstrated high power density and operational stability, producing over 2 mW cm^{-2} of power during 6 h of continuous operation. Recently, Li's group further advanced enzyme cascade research in MET-EBFCs by developing a hybrid enzymatic-organic cascade system consisting of an organic oxidation catalyst, 2,2,6,6-tetramethyl-1-piperidine N-oxyl (TEMPO), and an enzyme for bioelectronic applications.[83] In their design, TEMPO serves as both an oxidation catalyst and an electron mediator, allowing efficient electron transfer between the active center of the enzyme and the electrode surface. This MET-EBFC utilizing this system, with a Pt cathode, delivers a power density of 38.1 μW cm^{-2} under neutral pH, demonstrating the potential of this approach for bioelectronics and energy applications.

In 2014, Kwon et al. developed high-power MET-EBFC composed of GOx/poly(*N*-vinylimidazole)-[Os(4,4′-dimethoxy-2,2′-bipyridine)$_2$Cl])$^{+/2+}$-coated CNT yarn anode and BOD/PAA-poly(*N*-vinylimidazole)-[Os(4,4′-dichloro-2,2′-bipyridine)$_2$]$^{+/2+}$-coated CNT yarn cathode (**Figure 2a–c**).[48] These electrodes were fabricated by mixing enzyme solutions, Os-based redox polymers, a cross–linking agent, and a conducting polymer (poly(3,4-ethylenedioxythiophene), PEDOT). The resulting slurries were then used to coat CNT yarn electrodes. This fabrication approach significantly enhanced the electrochemical performance of electrodes. The electrochemical performance of the MET-EBFC was evaluated using anodic and cathodic current density measurements. A complete EBFC, featuring biscrolled anode and cathode yarns, generated an OCV of 0.70 V when operated in a 60 mmol L^{-1} oxygenated buffer. This result aligns with the potential difference observed for the onset of catalytic glucose oxidation at the anode (−0.30 V in Figure 2d) and catalytic oxygen reduction at the cathode (+0.50 V versus Ag/AgCl as shown in Figure 2e). These MET-EBFC electrodes exhibited impressive power performance, achieving 2.18 mW cm^{-2} with an OCV of 0.7 V (Figure 2f).

The robustness and versatility of these electrodes were further demonstrated by comparing the power density of the MET-EBFC in PBS) containing 7 mM glucose with that in human serum (Figure 2g). Despite the presence of potential interfering species in human serum, the CNT-based MET-EBFC maintained high power density, underscoring its potential for real-world applications, such as implantable EBFCs in physiological environments. The stability of the CNT yarn electrodes was also highlighted, where the power density of MET-EBFC remained consistent over several hours of operation (Figure 2h). Additionally, optical images at both low and high magnifications, of a 5 mm by 7 mm woven textile EBFC, featuring 50 mm diameter biscrolled yarn anodes and cathodes oriented in the warp direction, were presented in Figure 2i. These developments represent a significant advancement in MET-EBFC technology by utilizing CNT yarns as a robust platform for Os-based redox polymer/enzyme systems.

However, redox polymers containing heavy metal atoms, such as Os ions, may have adverse effects on living organisms when the polymeric chain dissociates. Therefore, several research groups have attempted to address this issue by using biocompatible organic catalysts such as ferritin (Frt), dopamine (DA), and vitamins.[60,84–86] For instance, Haque et al. fabricated a bioanode

© 2024 The Author(s). Advanced Functional Materials published by Wiley-VCH GmbH

16163028, 2025, 16, Downloaded from https://advanced.onlinelibrary.wiley.com/doi/10.1002/adfm.202415933 by Korea University Library, Wiley Online Library on [20/09/2026]. See the Terms and Conditions (https://onlinelibrary.wiley.com/terms-and-conditions) on Wiley Online Library for rules of use; OA articles are governed by the applicable Creative Commons License

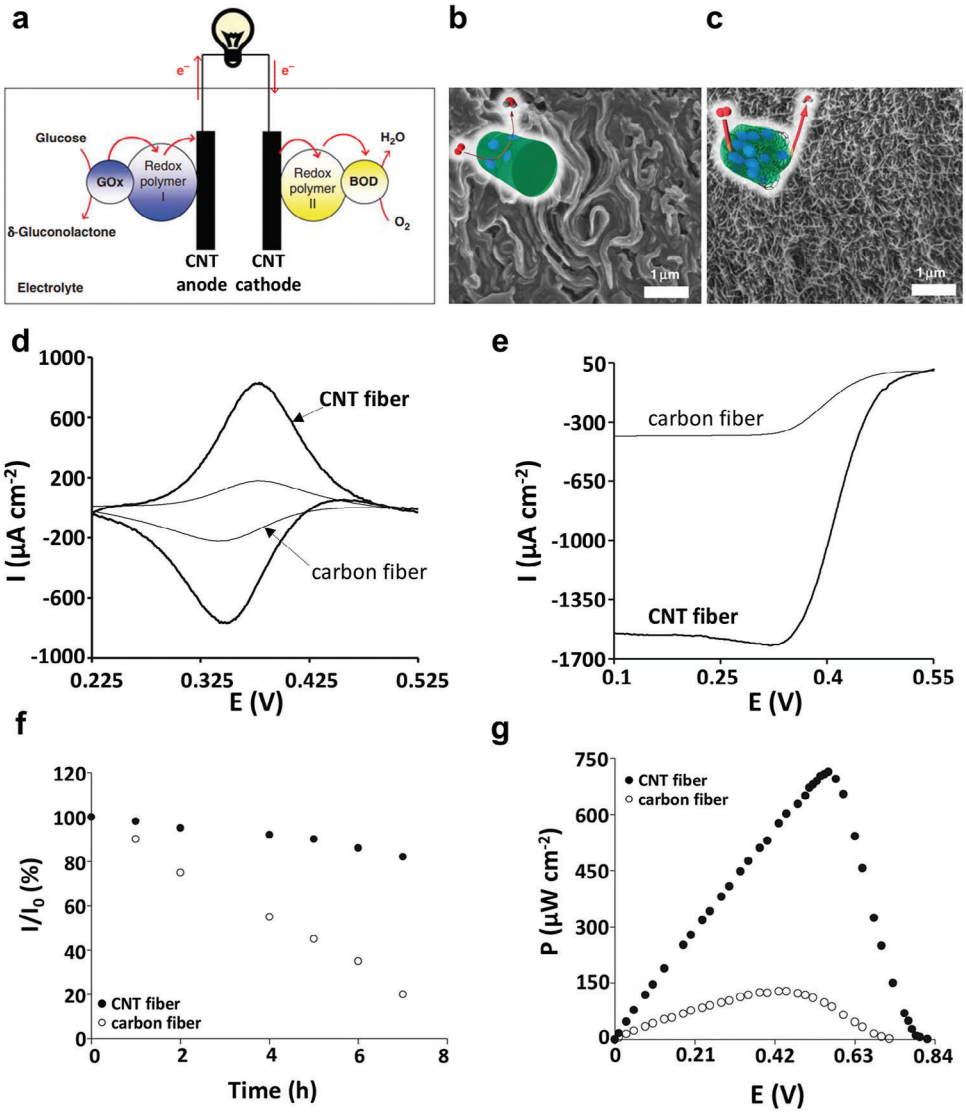

Figure 1. MET-EBFCs with Os-based redox mediators. a) Schematic of the BFC. At the anode, electrons are transferred from glucose to Gox, from GOx to redox polymer (I), and from (I) to the CNT fiber Reproduced with permission.[80] Copyright 2010, Springer Nature. b, c) SEM images illustrating the surface morphology of the carbon fiber cathode (b) and CNT fiber cathode (c) with a schematic indicating the electron flow and reactions occurring on the electrode surfaces (each inset). (the green shade represents redox polymer and the blue color the enzyme). Reproduced with permission.[80] Copyright 2010, Springer Nature. d) Dependence of current density (I) on voltage (V) for a CNT fiber (thick line) and a carbon fiber (thin line). Quiescent PBS buffer, under argon atmosphere at 37 °C, 20 mV s^{-1}, loading 170 µg. Reproduced with permission.[80] Copyright 2010, Springer Nature. e) Dependence of current density (I) on voltage (V) for a modified CNT fiber electrode (thick line) and a modified carbon fiber electrode (thin line). Quiescent phosphate-buffered saline buffer, under air at 37 °C, 5 mV s^{-1}, loading 170 µg. Reproduced with permission.[80] Copyright 2010, Springer Nature. f) Dependence of power density (P) on operating voltage (V) in a quiescent PBS buffer, under air, 15 mmol L^{-1} glucose at 37 °C, loading 226 µg. BFC made with carbon fiber (open circles) and CNT fiber (solid circles). Reproduced with permission.[80] Copyright 2010, Springer Nature. g) Dependence of relative stability (%) on time (h). PBS buffer at 37 °C, + 0.3 V versus Ag/AgCl, under 1 atm oxygen and vigorous stirring, loading 170 µg. BFC made of carbon fiber (open circles) and CNT fiber (solid circles). Reproduced with permission.[80] Copyright 2010, Springer Nature.

by immobilizing Frt and GOx with polythiophene-titanium dioxide (PTH-TiO_2) (**Figure 3a**).[87] The PTH-TiO_2-aided connection between Frt and the host electrode improved the electron transfer efficiency due to the increase in electrochemically active surface area by TiO_2 NPs and conductive polymer PTH (Figure 3b). The resulting PTH-TiO_2/Frt/GOx electrode demonstrated a notable current density of 7.8 ± 0.4 mA cm^{-2} when tested in a PBS solution containing 30 mmol L^{-1} glucose (Figure 3c,d). The CV scans were performed at various scan rates to assess the bioelectrocatalytic performance of the PTH-TiO_2/Frt/GOx bioanode, providing insights into FAD loading and electron transfer kinetics (Figure 3e). As the scan rate increased, the anodic and cathodic peaks shifted slightly with increasing scan rates, likely due to changes in the electrode layer; however, the formal potential of GOx remained stable. Clear redox peaks were observed, with a peak separation of 90 mV, indicating quasi-reversible

 © 2024 The Author(s). Advanced Functional Materials published by Wiley-VCH GmbH

16163028, 2025, 16, Downloaded from https://advanced.onlinelibrary.wiley.com/doi/10.1002/adfm.202415933 by Korea University Library, Wiley Online Library on [20/09/2026]. See the Terms and Conditions (https://onlinelibrary.wiley.com/terms-and-conditions) on Wiley Online Library for rules of use; OA articles are governed by the applicable Creative Commons License

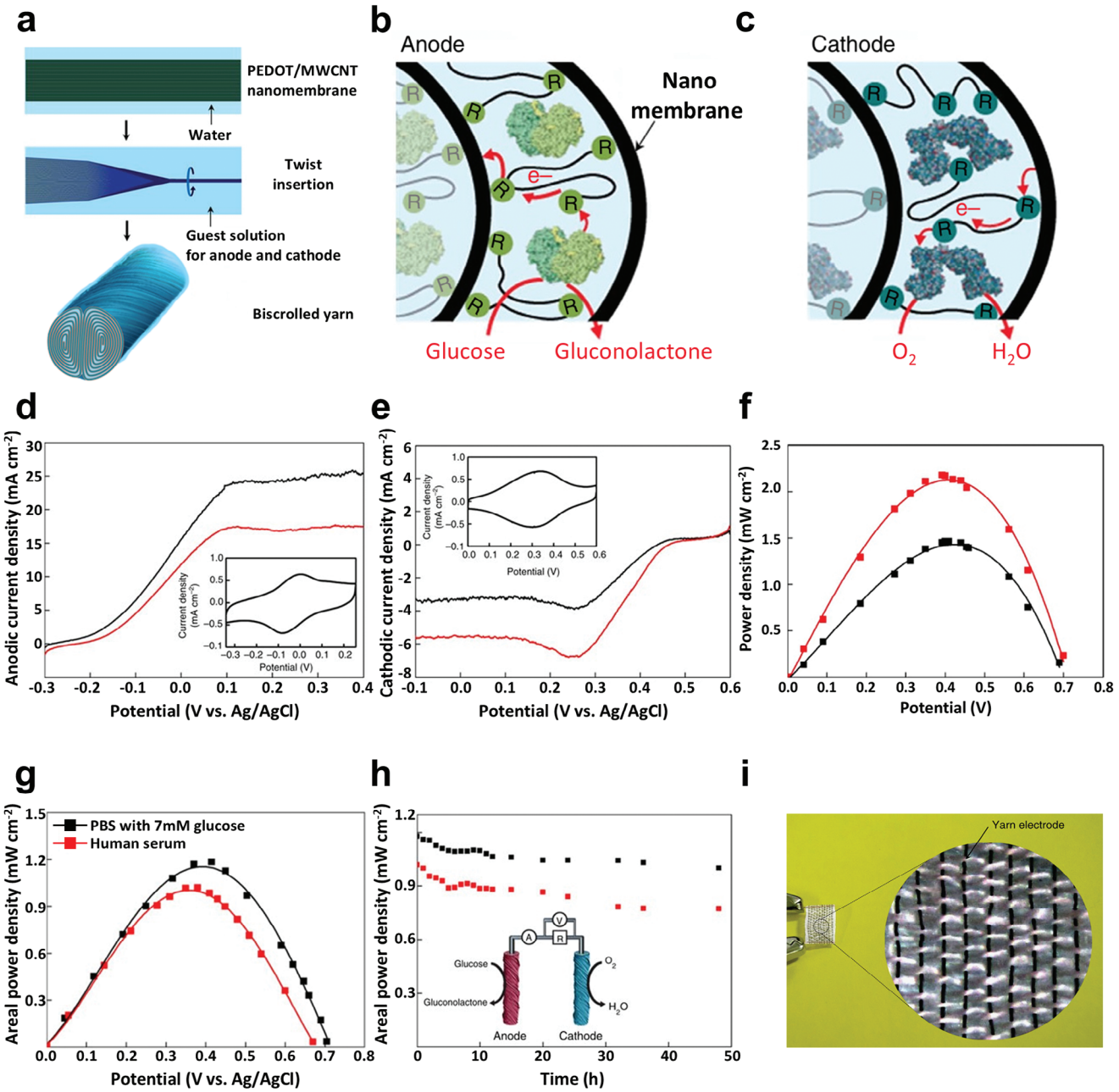

Figure 2. MET-EBFCs with Os-based redox mediators. a) Schematic illustration of the fabrication method for biscrolled yarn electrodes. Reproduced with permission.[48] Copyright 2014, Springer Nature. b,c) Schematic illustration of the structure and function of BFC electrode yarns, indicating the associated electron transfer processes and chemical transformations. The enzyme and redox mediator used in the anode were GOx and mediator I (b), and in the cathode were BOD and mediator II (c). Reproduced with permission.[48] Copyright 2014, Springer Nature. d) Polarization curves for the BFC yarn anode at 60 mmol L^{-1} glucose concentration. Inset: CV curve showing the peak of redox polymer I for anode under argon. Reproduced with permission.[48] Copyright 2014, Springer Nature. e) Polarization curve for the BFC yarn cathode at 60 mmol L^{-1} glucose concentration. Inset: CV showing the peak of redox polymer II for cathode under argon. Reproduced with permission.[48] Copyright 2014, Springer Nature. f) Areal power density as a function of potential for the complete BFC system at 60 mmol L^{-1} glucose concentration. Reproduced with permission.[48] Copyright 2014, Springer Nature. d-f) The experiment was carried out under 20 mmol L^{-1} PBS solution (temperature: 37 °C, scan rate: 5 mV s^{-1}), when saturated with air (black symbols and curves) and O_2 (red symbols and curves). g) Areal power density as a function of cell voltage for a biscrolled yarn BFC. Reproduced with permission.[48] Copyright 2014, Springer Nature. h) Dependence of areal power output on time for a biscrolled yarn BFC (poised at 0.40 V). Inset: illustrates the redox processes and indicates the resistance (R) of the applied external load and the location of voltage (V) and current (A) measuring devices. Reproduced with permission.[48] Copyright 2014, Springer Nature.

 © 2024 The Author(s). Advanced Functional Materials published by Wiley-VCH GmbH

16163028, 2025, 16, Downloaded from https://advanced.onlinelibrary.wiley.com/doi/10.1002/adfm.202415933 by Korea University Library, Wiley Online Library on [20/09/2026]. See the Terms and Conditions (https://onlinelibrary.wiley.com/terms-and-conditions) on Wiley Online Library for rules of use; OA articles are governed by the applicable Creative Commons License

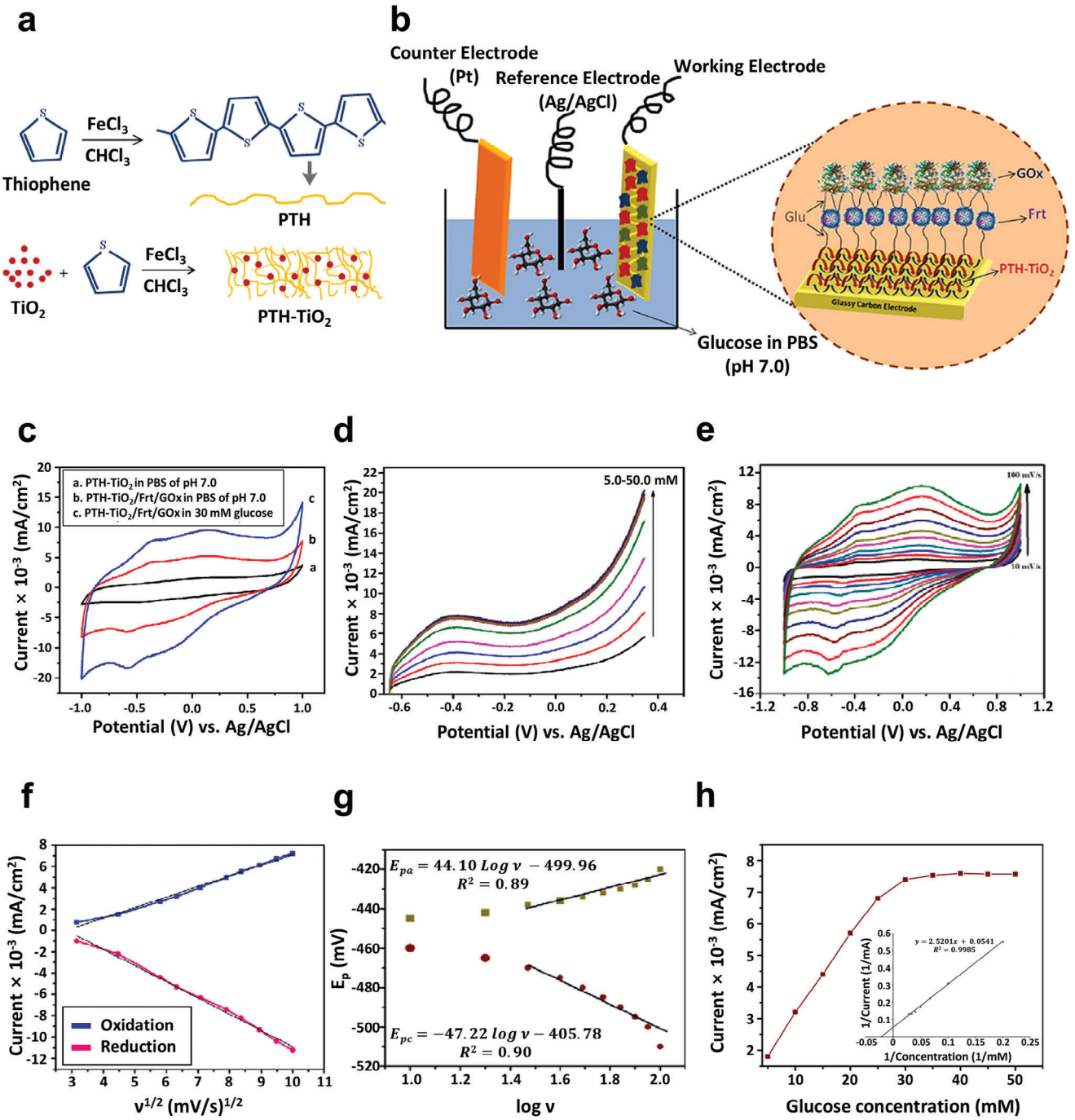

Figure 3. MET-EBFCs with biomolecule-based redox mediators. a) Schematic drawing of synthetic route for PTH and PTH-TiO_2 composite. Reproduced with permission.[87] Copyright 2022, Elsevier. b) Pictorial presentation of the PTH-TiO_2/Frt/GOx bioanode. Reproduced with permission.[87] Copyright 2022, Elsevier. c) CV for a. PTH-TiO_2 in PBS of pH 7.0, b. PTH-TiO_2/Frt/GOx in PBS of pH 7.0, c. In 30 mmol L^{-1} glucose dissolved in PBS of pH. 7.0. Reproduced with permission.[87] Copyright 2022, Elsevier. d) Polarization curves at different glucose concentrations ranging from 5 to 50 mmol L^{-1}. Reproduced with permission.[87] Copyright 2022, Elsevier. e) CV investigations for PTH-TiO_2/Frt/GOx at various scan rates (10–100 mV s^{-1}) in 30 mM glucose substrate dissolved in PBS (pH 7.0). Reproduced with permission.[87] Copyright 2022, Elsevier. f) Graph of current versus $\nu^{1/2}$. Reproduced with permission.[87] Copyright 2022, Elsevier. g) Graph of E_p versus log ν. Reproduced with permission.[87] Copyright 2022, Elsevier. h) Plot of current versus glucose concentration (5–50 mM) with inset of Lineweaver Burk plot for K_m^{app} determination. Reproduced with permission.[87] Copyright 2022, Elsevier.

 © 2024 The Author(s). Advanced Functional Materials published by Wiley-VCH GmbH

16163028, 2025, 16, Downloaded from https://advanced.onlinelibrary.wiley.com/doi/10.1002/adfm.202415933 by Korea University Library, Wiley Online Library on [20/09/2026]. See the Terms and Conditions (https://onlinelibrary.wiley.com/terms-and-conditions) on Wiley Online Library for rules of use; OA articles are governed by the applicable Creative Commons License

electron transfer. The redox currents increased linearly with increasing scan rate, suggesting a surface-controlled process, while a linear relationship between the current density and the square root of scan rate ($v^1/^2$) indicated a combination of diffusion and surface-controlled oxidation (Figure 3f). The heterogeneous electron transfer rate constant (k_s) for GOx at the PTH-TiO_2/Frt/GOx bioanode was estimated, with a slope of 44.10 mV, confirming efficient electron transfer kinetics in the system (Figure 3g). The relationship between current and glucose concentration exhibited an initial linear increase up to 30 mmol L^{-1} glucose, consistent with first-order kinetics (Figure 3h). Beyond this concentration, the current saturated, indicating zero-order kinetics. The system reached equilibrium at a current density of 7.4 ± 0.4 mA cm^{-2}, demonstrating efficient bioelectrocatalytic performance at optimal glucose concentrations.

However, despite the advances in electrochemical technology and the commendable power performance of MET-EBFCs, serious concerns remained about their potential toxicity and operational instability, mainly due to mediator leaching, and the complex synthesis of mediators. More recently, Inammuddin and coworkers developed a polypyrrole (PPy)-based EBFC anode using vitamin K_3 (VK_3) as a redox mediator, which has a lower oxidation potential than Frt.[88] To control the size and morphology of the PPy, a cationic surfactant (cetyltrimethylammonium bromide, CTAB) was employed as a structural-directing agent. The proposed anode system (i.e., PPy/CTAB/VK_3/GOx) exhibited an areal current density of 6.35 mA cm^{-2} in a 20 mmol L^{-1} glucose solution. However, the specific performance of the power output and operational stability of the complete cell system was not reported, as no cathode was included in the study. To address issues related to mediator synthesis and leaching, significant research has focused on enhancing electron transfer, power performance, and operational stability in mediator-free EBFCs (DET-EBFCs). The following section provides an overview of these research efforts.

2.2.2. Glucose-based DET-EBFCs

In DET-EBFCs, the enzymes transfer electrons directly to the host electrode, without any intermediate. Particularly, the DET in glucose-based EBFCs using GOx has been a subject of ongoing investigation due to its structural limitations.[89,90] Specifically, the redox center of GOx is deeply embedded within the enzyme, which restricts DET to the surface of the electrode. Despite these limitations, GOx is still widely used in various applications such as blood glucose monitoring due to its high specificity and stability. Several studies have investigated the use of carbon-based materials, such as CNTs and graphene, to improve the electrochemical response of GOx, indicating that these materials could facilitate DET.[91–93] Given the unique advantages of GOx, there is growing interest in exploring DET in EBFCs. As a result, research in this area remains highly active, focusing on GOx, other enzymes like GDH, and enzyme cascade methods. For example, the Bollella group successfully demonstrated the use of pyrroloquinoline quinone (PQQ)-dependent GDH (PQQ-GDH) in a DET-EBFC designed for implantable devices.[94] In their study, PQQ-GDH was immobilized on buckypaper electrodes to catalyze glucose oxidation, while BOD was used at the cathode for oxygen reduction. The resulting DET-EBFC generated sufficient power ranging from 2 to 10 µW, depending on the glucose concentration and the medium used (aqueous or hemolymph), to operate a microelectronic sensor in a biological environment, such as within a slug. This research highlights the potential of PQQ-GDH-based DET-EBFCs for small-scale, energy-autonomous devices, particularly in biomedical implants.

Another notable approach involves the development of bi-enzyme-based BFCs to overcome the limitations associated with GOx. For instance, Chung and colleagues constructed a bi-enzyme system incorporating both GOx and horseradish peroxidase (HRP) with terephthaladehyde as a cross–linking agent.[95] In the glucose oxidation process, the reduction of FAD in GOx to $FADH_2$ leads to the production of H_2O_2, which acts as an inhibitor of GOx and can impede the overall reaction. To address this issue, HRP was included to break down the H_2O_2, thereby ensuring the continued functionality of the enzyme. This bi-enzyme approach resulted in a power density of 2.1 mW cm^{-2}, with the power output maintaining ≈85% of its original value after 20 days of periodic measurements. This demonstrates how the incorporation of multiple enzymes in a cascade reaction can enhance the performance of DET-EBFCs by mitigating challenges such as enzyme inhibition.

Although these DET-EBFCs offer several advantages over MET-EBFCs, such as the simplified electrode structure, the use of non-toxic components, and enhanced stability, they still face significant limitations. A major challenge is their low electron transfer efficiency, which results from direct electron tunneling between the host electrode and the active site of the enzyme. This issue is particularly pronounced for electrically poor enzymes and can restrict both the thickness of the enzyme layer and the amount of enzyme loading, thereby limiting the areal power output of DET-EBFCs. Additionally, DET can lead to slow reaction rates at the electrode, reducing the overall efficiency of the EBFC system. Furthermore, the dependence on specific electrode materials restricts material selection, complicating commercialization efforts, and the unstable voltage output can hinder continuous power supply. Despite these challenges, recent reports have highlighted significant progress in overcoming these barriers, with several approaches contributing to the advancement of DET-EBFCs.

A few research groups utilized metal NPs to enhance the electron transfer between the host electrode and enzymes by leveraging the electron relay effect. For instance, Huang et al. used a novel approach in which electrostatically charged Au NPs were uniformly deposited on laser-induced graphene (LIG), and then GOx and Lac were additionally deposited for the anode and cathode, respectively (**Figure 4a**).[96] The configuration of the bioanode and biocathode arrays is illustrated with an optical image of the transient, implantable, ultrathin DET-EBFC device (Figure 4b,c). The resulting EBFC electrodes of the complete cell exhibited promising characteristics, including a relatively low impedance (16 Ω) (Figure 4d). The anode demonstrated a clear increase in current with increasing glucose concentrations, highlighting its sensitivity (Figure 4e). As a result, the maximum power output of the assembled EBFCs based on the electrodes of LIG and LIG/Au NPs composite reached 483.1 µW cm^{-2}, with an OCV of 0.77 V (Figure 4f). Additionally, the chronoamperometric response demonstrated a rapid and stable potential change upon

© 2024 The Author(s). Advanced Functional Materials published by Wiley-VCH GmbH

16163028, 2025, 16, Downloaded from https://advanced.onlinelibrary.wiley.com/doi/10.1002/adfm.202415933 by Korea University Library, Wiley Online Library on [20/09/2026]. See the Terms and Conditions (https://onlinelibrary.wiley.com/terms-and-conditions) on Wiley Online Library for rules of use; OA articles are governed by the applicable Creative Commons License

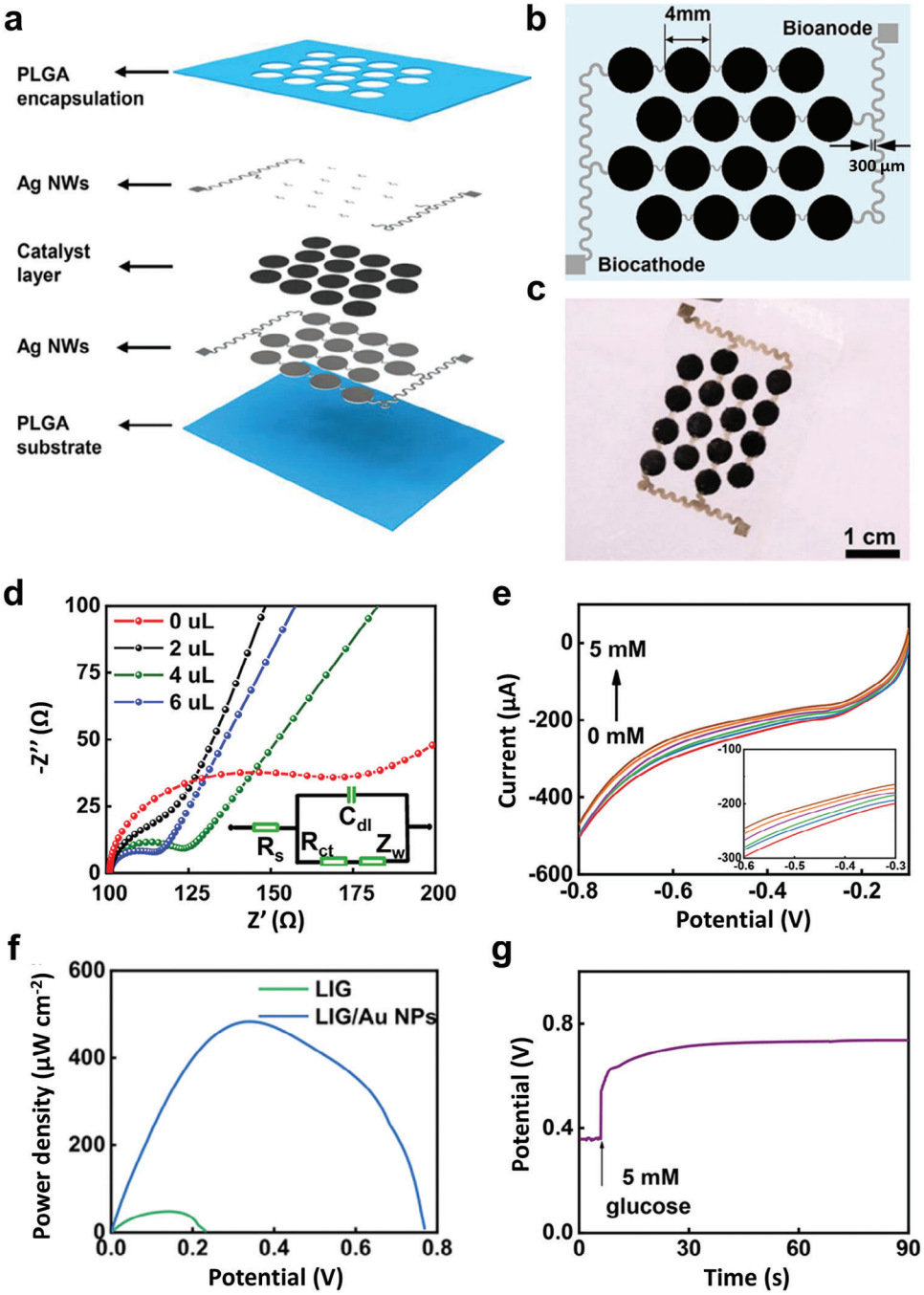

Figure 4. DET-EBFCs. a) Schematic illustration of an EBFC array based on the LIG/Au NPs composite. Reproduced with permission.[96] Copyright 2022, American Chemical Society. b) Design sketch of the EBFCs. Reproduced with permission.[96] Copyright 2022, American Chemical Society. c) Optical image of the EBFCs. Reproduced with permission.[96] Copyright 2022, American Chemical Society. d) EIS of the LIG electrode and the LIG/Au NPs electrodes with 2, 4, and 6 μL of $HAuCl_4$. Reproduced with permission.[96] Copyright 2022, American Chemical Society. e) LSV curves of the bioanode in the PBS solution containing 0–5 mM glucose. Reproduced with permission.[96] Copyright 2022, American Chemical Society. f) Comparison of maximum power density for EBFCs based on LIG and LIG/Au NPs composite. Reproduced with permission.[96] Copyright 2022, American Chemical Society. g) Activation performance of the EBFC. Reproduced with permission.[96] Copyright 2022, American Chemical Society.

glucose introduction, confirming the stability of the system and the fast electron transfer capabilities (Figure 4g). This system also exhibited an impressive operational lifetime, exceeding 28 days in vitro. Overall, this innovative DET-EBFC design shows great promise for flexible and efficient EBFC applications.

However, the integration of electrostatically charged metal NPs with enzymes in aqueous electrolytes has often relied on conventional methods such as reconstitution, physical adsorption, and mechanical mixing. While these approaches using metal NPs hold the potential to facilitate favorable enzyme wiring for

 © 2024 The Author(s). Advanced Functional Materials published by Wiley-VCH GmbH

16163028, 2025, 16, Downloaded from https://advanced.onlinelibrary.wiley.com/doi/10.1002/adfm.202415933 by Korea University Library, Wiley Online Library on [20/09/2026]. See the Terms and Conditions (https://onlinelibrary.wiley.com/terms-and-conditions) on Wiley Online Library for rules of use; OA articles are governed by the applicable Creative Commons License

DET, they encounter challenges in significantly enhancing electron transfer due to various contact resistances. These resistances primarily stem from electrically or electrochemically inactive organic compounds, such as organic ligands and cross–linkable polymers, as well as the low packing density of electrostatically charged metal NPs due to electrostatic repulsion in water.[97,98] Furthermore, the resulting enzyme electrodes often suffer from ineffective enzyme immobilization due to insufficient interfacial interactions between the electrode components, leading to compromised operational stability.

Another effective strategy involves using the 3D porous host electrode with a high surface area, such as CNT yarns, metal foams, and conductive textiles. This approach enhances the enzyme loading capacity and improves the electron transfer efficiency through their conductive porous structure, resulting in a significant increase in power performance per unit area. Among these porous host electrodes, CNT yarns or CNT-coated textiles offer specific advantages, including pore diameter control, lightweight properties, and relatively high electrical conductivity. For instance, the Cosnier group reported the efficient wiring of GOx and Lac in a multi-walled CNT (MWCNT) matrix to create an EBFC.[99] GOx and Lac were incorporated into compressed MWCNT disks to form the anode and cathode, respectively (**Figure 5a**). FE-SEM analysis of the bioelectrodes revealed well-dispersed enzyme agglomerates throughout the CNT matrix, as illustrated in the cross–section image of the bioanode (Figure 5b). The MWCNT bioelectrodes exhibited a high surface area of 180 $m^2\ g^{-1}$ and a porosity of 43%, both of which are favorable for bioelectrocatalysis. To optimize the cathode performance, various amounts of Lac were incorporated into the CNT disks. With increasing Lac load, the electrode resulted in generating higher current density at 0 V and stabilized the current density at −5.8 mA cm^{-2} (Figure 5c). The stability of the cathode was evaluated over 30 days, with the OCP and current density remaining stable after an initial decrease, maintaining values of 0.55 V and 3.8 mA cm^{-2}, respectively (Figure 5d).

Next, the effect of the catalase-to-GOx ratio on the anode was investigated (Figure 5e). Increasing this ratio improved current density, reaching a maximum of 4.8 mA cm^{-2}, while the open circuit potential (OCP) stabilized at −0.43 V, indicating effective decomposition of H_2O_2 and efficient electron transfer between GOx and the CNT matrix. The anode demonstrated good stability, with only a 25% reduction in current after 30 days and a minor positive shift in OCP (Figure 5f). To demonstrate the practical application of the EBFC, two cells were connected in series, producing an OCV of 1.8 V and a maximum power output of 3.25 mW at 1.2 V, sufficient to power electronic devices (Figure 5g). Additionally, during a constant current discharge of 200 μA cm^{-2} for 8000 s, the voltage dropped to 0.6 V, but the cell maintained the current discharge (Figure 5h).

However, despite these endeavors to improve the areal power density and stability, most DET-EBFCs fall short of meeting practical and commercial performance. It should also be noted that the EBFC electrode components (i.e., enzymes, binder, and/or conductive components) coated by the slurry casting process are highly prone to enzyme leaching.[30,42] Given this challenge, there is an urgent need to develop a more effective deposition process, along with a unique structural and interfacial design for high-performance EBFC electrodes. If successfully implemented, such an innovative approach can have the potential to surpass the power performance and operational stability of traditional MET-EBFCs reported to date. A detailed exploration of this promising advancement is provided in Section 3.

2.2.3. Electron Transfer Measurements of Glucose-based EBFCs

As previously discussed, the electron transfer efficiency of EBFCs plays a pivotal role in determining the power performance of both MET- and DET-EBFCs. Therefore, conducting the precise investigation and measurement of various factors and parameters closely associated with the electron transfer efficiency of EBFCs can provide valuable insights for predicting and enhancing the power density and stability of these cells.

Representative parameter values, such as the equivalent series resistance (R_s), the electron charge transfer resistance (R_{ct}), and the k_s are evaluated using both the electrochemical impedance spectroscopy (EIS) and the Laviron equation.[100–102] These values strongly rely on the ease of electron transfer between the enzyme and the host electrode.

Initially, the R_s value is determined by summing up the resistance originating from each electrode component, including the electrolyte, the active components (enzyme, conductive component, and/or mediator), the host electrode, and the interfaces, mainly those between the active components and the host electrode. In addition, the R_{ct}, which occurs mainly at the interface between the active material and the electrolyte, is significantly influenced by the geometric properties and surface chemistry of the entire electrode. Thus, the decrease in R_s and R_{ct} values in the enzymatic electrode implies an improvement in the electron transfer efficiency of the entire electrode, encompassing the electron transfer between the enzymes and the host electrode. For example, Huang et al. demonstrated the successful employment of PPy network growth to encapsulate the GOx for self-encapsulation of glucose.[103] In this case, the observed reductions in R_s and R_{ct} values are indicative of the accelerated electron transfer rates facilitated by the conductive PPy network. These results underscore the effectiveness of conductive polymer shells in promoting electron transfer within the enzymatic electrode.

In addition, the Laviron equation serves as a model for calculating the electron transfer coefficient (α) and the k_s value of oxidizing and reducing species on the electrode surface. These parameters are crucial in determining the electrochemical behavior of the electrode. Typically, the redox reaction of a component triggered by a potential sweep may exhibit irreversibility, depending on the direction of the applied potential. This theoretical concept is expressed by the following equations (Equations 4–9):

$$\Delta E_{pc} = -\frac{RT}{\alpha nF}\ \ln\left(\frac{\alpha}{|m|}\right) = -\frac{RT}{\alpha nF}\ \ln\left(\nu\frac{\alpha nF}{RTk_s}\right) = -\frac{RT}{\alpha nF}\ln(\nu) - \frac{RT}{\alpha nF}\ \ln\left(\frac{\alpha nF}{RTk_s}\right) = a_c\ x + b_c \quad (4)$$

$$a_c = -\frac{2.303RT}{\alpha nF},\quad \mathrm{b}_c = -\frac{2.303RT}{\alpha nF}\log\left(\frac{\alpha nF}{RTk_s}\right),\ x = \log(\nu) \quad (5)$$

© 2024 The Author(s). Advanced Functional Materials published by Wiley-VCH GmbH

16163028, 2025, 16, Downloaded from https://advanced.onlinelibrary.wiley.com/doi/10.1002/adfm.202415933 by Korea University Library, Wiley Online Library on [20/09/2026]. See the Terms and Conditions (https://onlinelibrary.wiley.com/terms-and-conditions) on Wiley Online Library for rules of use; OA articles are governed by the applicable Creative Commons License

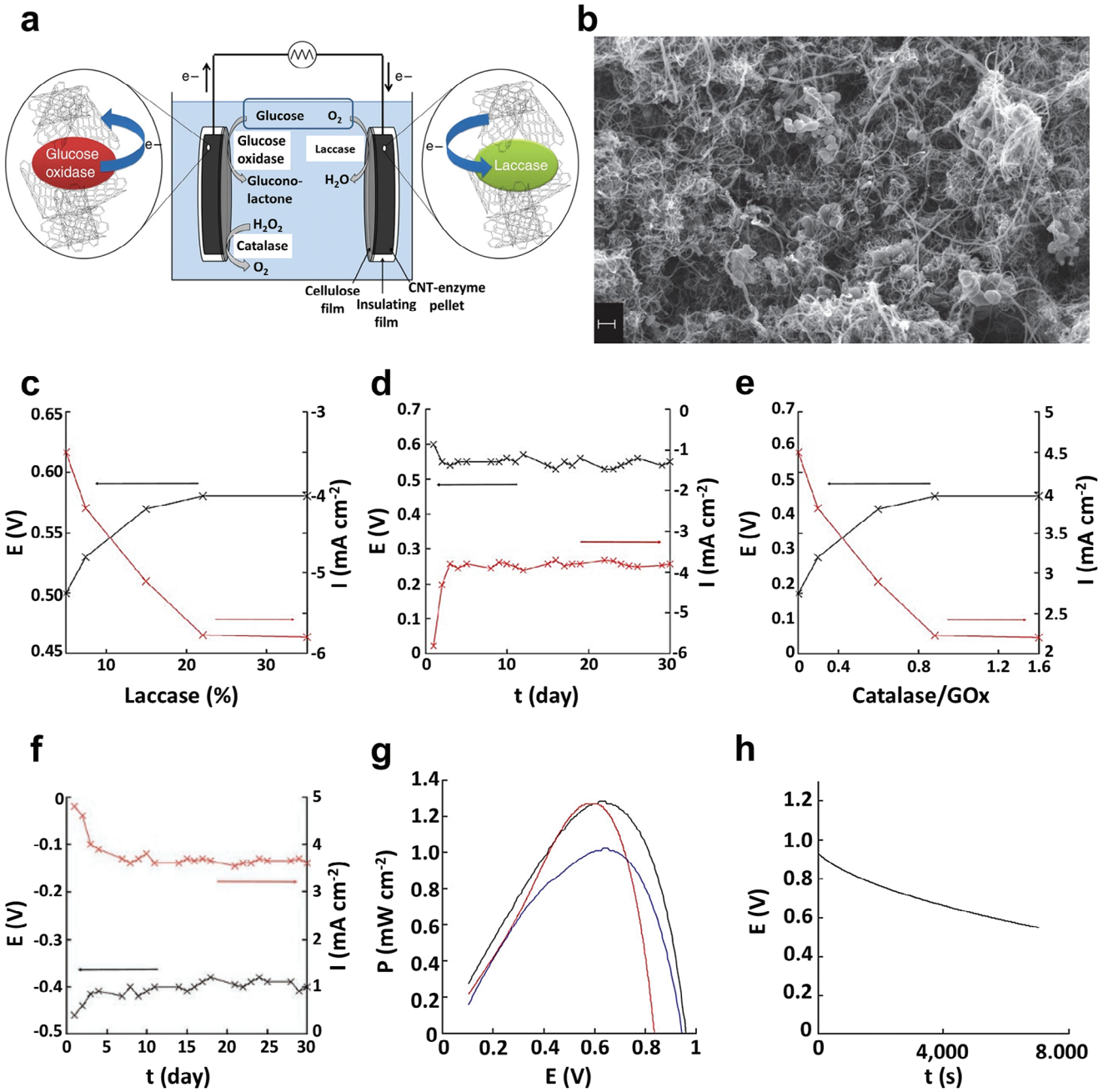

Figure 5. DET-EBFCs. a) Schematic presentation of the setup of a BFC. Reproduced with permission.[99] Copyright 2011, Springer Nature. b) SEM micrograph of a cross–section of the bioanode. The scale bar corresponds to 200nm. Reproduced with permission.[99] Copyright 2011, Springer Nature. c) Evolution of OCP (black) and current density (red) at 0 V, with different amounts of laccase (mass percentage in the electrode) in air-saturated solution. Reproduced with permission.[99] Copyright 2011, Springer Nature. d) Evolution of OCP (black) and current density (red) at 0 V, of biocathode (20% laccase) versus time. Reproduced with permission.[99] Copyright 2011, Springer Nature. e) Evolution of OCP (black) and current density (red) at 0 V, versus catalase/GOx ratio in bioanode, in 0.05 mol L^{-1} glucose solution. Reproduced with permission.[99] Copyright 2011, Springer Nature. f) Evolution of OCP (black) and current density (red) of bioanode (catalase/GOx ratio 1:1) at 0 V versus time, in 0.05 mol L^{-1} glucose solution. Reproduced with permission.[99] Copyright 2011, Springer Nature. g) Dependence of power density on operating voltage in 0.05 mol L^{-1} glucose solution before (black) and after one month (red). Blue curve: dependence of power density on operating voltage in 5×10^{-3} mol L^{-1} glucose. Reproduced with permission.[99] Copyright 2011, Springer Nature. h) Dependance of voltage on time for continuous discharge under 200 μA cm^{-2} in 0.05 mol L^{-1} glucose solution. Reproduced with permission.[99] Copyright 2011, Springer Nature.

 © 2024 The Author(s). Advanced Functional Materials published by Wiley-VCH GmbH

16163028, 2025, 16, Downloaded from https://advanced.onlinelibrary.wiley.com/doi/10.1002/adfm.202415933 by Korea University Library, Wiley Online Library on [20/09/2026]. See the Terms and Conditions (https://onlinelibrary.wiley.com/terms-and-conditions) on Wiley Online Library for rules of use; OA articles are governed by the applicable Creative Commons License

$$\Delta E_{pa} = \frac{RT}{(1-\alpha)\,nF}\ \ln\left(\frac{(1-\alpha)}{m}\right) = \frac{RT}{(1-\alpha)\,nF}\ \ln\left(\nu\frac{(1-\alpha)\,nF}{RTk_s}\right) = \frac{RT}{(1-\alpha)\,nF}\ \ln(\nu) + \frac{RT}{(1-\alpha)\,nF}\ \ln\left(\frac{(1-\alpha)\,nF}{RTk_s}\right) = a_a\,x + b_a \quad (6)$$

$$a_a = \frac{2.303RT}{(1-\alpha)\,nF}\ ,\quad \mathrm{b}_a = \frac{2.303RT}{(1-\alpha)\,nF}\ \log\left(\frac{(1-\alpha)\,nF}{RTk_s}\right),\quad x = \log(\nu) \quad (7)$$

$$\Delta \mathrm{E}\ = E_{pc}\ - E^{\circ}\ \text{or}\ \ E_{pa} - E^{\circ} \quad (8)$$

$$\log\ k_s = \alpha\log(1-\alpha) + (1-\alpha)\log\alpha - \log(\frac{RT}{nF\nu}) - \frac{\alpha\,(1-\alpha)\,nF\Delta E}{2.303RT} \quad (9)$$

The Laviron model for redox substances employs various variables, including universal gas constant (R ~8.314 J mol^{-1} K^{-1}), absolute temperature (T), charge transfer coefficient (α), heterogeneous electron transfer rate constant (k_s), Faraday constant (F ~96 485 C), anodic peak potential (E_{pa}), cathodic peak potential (E_{pc}), apparent formal redox potential (E°), number of electrons transferred (n ~1), anodic curve slope (a_a), anodic curve intercept (b_a), cathodic curve slope (a_c), cathodic curve intercept (b_c), scan rate (ν), and logarithm of scan rate (x). These variables are utilized in the generalization of the Laviron model. Furthermore, the k_s value can be determined by analyzing the intersection of two linear fits corresponding to the anodic and cathodic curves.

This k_s value has long been recognized as a crucial parameter for elucidating the kinetics of the electron transfer process at the electrode surface. In particular, this parameter signifies the rate at which the electrochemical enzymatic reaction takes place at the electrode surface under standard conditions, typically at room temperature (25 °C) and at a standard reactant concentration. It determines the rate at which the enzymatic reaction occurs at the surface of an EBFC electrode. Therefore, an increased k_s value directly indicates the improved electron transfer efficiency of EBFC electrodes. For instance, the k_s value of the mediator-free enzymatic anode composed of GOx and rGO was estimated to be ≈2.14 s^{-1}.[36] However, when the synthesized electrocatalysts (i.e., Meldola's Blue) were integrated with mesoporous carbons (highly conductive components) or CNTs onto glassy carbon-based host electrode, the resulting anodes exhibited significantly higher k_s values of ≈39.8 and 9.8 s^{-1}, respectively, exceeding that of the aforementioned GOx/rGO-based anode.[104] As a result, the k_s value not only provides insight into the electron transfer kinetics of the electrode but also enhances the understanding of the relationship between the electron transfer kinetics and the current/power density of the electrodes, thereby improving the efficiency of the DET-EBFC system.

2.3. Enzyme Immobilization for Glucose-based EBFCs

Enzyme immobilization is a critical technique for fabricating high-performance EBFCs because immobilized enzymes are more stable than their free counterparts. This stability results in longer operational lifetimes, reduced degradation, and enhanced enzymatic activity due to the creation of a more favorable microenvironment. Notably, the detachment of enzymes from the host electrode is a key factor that significantly affects the operational stability of EBFCs.

First, we examine various approaches for enzyme immobilization and assess their impact on electron transfer within EBFCs. As shown in **Table 1**, one approach involves adsorption, where enzymes adhere to electrode surfaces through weak interactions such as van der Waals forces and hydrogen bonding.[105–107] While adsorption is a straightforward and effective method for immobilizing enzymes at the enzyme-host electrode interface, it may not ensure robust adsorption between adjacent enzyme layers as the thickness of immobilized enzymes increases. On the other hand, covalent bonding can establish relatively strong bonds between enzymes and host electrodes, offering improved stability and reusability.[2] For example, Moon and colleagues reported the covalent bonding-induced immobilization of amine-terminated GOx (NH_2-GOx) onto a ferrocene derivative (FcDA)-modified graphite carbon felt to form the anode.[108] Similarly, BOD was covalently immobilized on acid-treated graphite carbon felt to form the cathode. However, this covalent bonding approach has a critical problem: the formation of 1-ethyl-3-(3-dimethylaminopropyl)carbodiimide (EDC)/*N*-hydroxysuccinimide (NHS)-induced covalent bonds between NH_2-GOx and FcDA can partially cause enzyme denaturation and/or loss of activity due to the harsh chemical conditions required for covalent bond formation. Another enzyme immobilization method, cross–linking approach, involves the covalent attachment of enzymes to electrode surfaces using bi- or multifunctional agents such as poly (ethylene glycol) diglycid (PEGDGE), glutaraldehyde, or carbodiimide.[109–111] While this method achieves strong enzyme immobilization, the formation of large aggregates can impede the electrical conductivity of the electrode.

In contrast to the aforementioned adsorption and cross–linking approaches, the encapsulation/entrapment approach involves the physical entrapment within polymer matrices or membranes, providing both protection and physiological stabilization. Although these methods are commonly used to immobilize enzymes onto host electrodes for prolonged use under harsh conditions, they are limited in their ability to significantly enhance the energy efficiency of EBFCs due to diffusion constraints and reduced enzyme activity within the matrix. As a result, these conventional immobilization methods exhibit limitations in electron transfer efficiency and mass transport within the electrodes, emphasizing the need for advanced immobilization techniques to optimize EBFC electrode fabrication.[106]

Another approach to enzyme immobilization involves the use of nanomaterial-based covalent bonding, which is known to substantially enhance the operational stability of EBFC electrodes. Of particular note is the combination of electrically and/or electrochemically active nanomaterials with enzymes through favorable complementary interactions, leading to a significant improvement in the electron transfer efficiency between host electrodes and enzymes, thereby enhancing the electrochemical performance of the resulting electrodes.[41,112] For example, carbon-based nanomaterials, predominantly CNTs and reduced graphene oxides (rGO), with high electrical conductivity and electrochemical stability, are effective in immobilizing enzymes.[56] This results in electrodes with high electron transfer efficiency, which is beneficial for the fabrication of

© 2024 The Author(s). Advanced Functional Materials published by Wiley-VCH GmbH

16163028, 2025, 16, Downloaded from https://advanced.onlinelibrary.wiley.com/doi/10.1002/adfm.202415933 by Korea University Library, Wiley Online Library on [20/09/2026]. See the Terms and Conditions (https://onlinelibrary.wiley.com/terms-and-conditions) on Wiley Online Library for rules of use; OA articles are governed by the applicable Creative Commons License

Table 1. Advantages/disadvantages and examples of enzyme immobilization methods.

Immobilization method	Advantages	Disadvantages	Example	Refs.
Adsorption	• Simplicity, cost-effectiveness • Minimal chemical modification required	• Weak enzyme binding may lead to leaching. • Limited control over enzyme orientation	Fructose dehydrogenase on cellulose/PPy	[107]
Covalent bonding	• Strong, stable enzyme attachment • Improved control over enzyme orientation	• Chemical modification may cause denaturation/loss of enzyme activity. • Labor-intensive and costly	GOx, ferrocene derivative on a graphite carbon felt	[108]
Cross–linking	• Enhanced stability through enzyme clustering • Reduced leaching	• Cross–linking agents may affect enzyme activity. • Limited control over cross–linking density	GOx, Os-based mediator with PEGDGE	[109]
Encapsulation /Entrapment	• Protection against environmental factors • Increased stability	• Diffusion limitations may affect substrate access. • Limited control over enzyme orientation	PPy network for encapsulation of GOx	[103]
Layer-by-Layer assembly	• Preservation of enzyme stability and activity • High compatibility with a wide range of materials	• Production process may be complicated. • High cost of materials	GA/[[GOx/PEI]$_2$/CNTs] as bioanodes, GA[Lac/PEI/Lac/CNTs] as biocathodes	[117]

high-performance biosensors or EBFCs.[113,114] However, despite these efforts, the operational stability of most EBFCs remained unsatisfactory, with power output often dropping below 50% of the initial value at a glucose concentration of 10 mmol L^{-1}—close to physiological conditions—after just 10 to 20 days.

Additionally, an enzyme immobilization for enhanced operational stability can be achieved by an electrostatic LbL assembly, which is based on electrostatic interaction between electrostatically charged enzyme and oppositely charged component in aqueous media on the host electrode.[115–118] This LbL assembly approach can be easily applied to various substrates irrespective of their size and shape. For example, Hyun et al. reported that (anionic GOx/cationic poly(ethylene imine) (PEI))$_n$ multilayers were deposited onto MWCNT using electrostatic interaction, resulting in the stable operation.[117] However, the use of insulating polyelectrolytes can significantly restrict the electron transfer between adjacent enzymes as well as between the host electrode and enzyme.

Recently, an innovative enzyme immobilization method has emerged to boost the power density and operational stability of EBFCs. Unlike conventional LbL assemblies using insulating polyelectrolytes in aqueous media, this approach utilizes direct ligand exchange reaction (LER) bulky insulating ligands initially bound to the surface of conductive NPs and NH_2 groups of enzymes like GOx or small organic molecules, which are evidently different from conventional LbL assembly without LER. This reaction facilitates the direct contact between highly conductive NPs and enzymes, significantly improving the electron transfer between adjacent GOx as well as between the host electrode and GOx. Furthermore, LER-LbL assembly is effective in fabricating highly conductive host electrodes.[119–121] It transforms insulating porous substrates into highly conductive host electrodes through an LER between bulky ligands on the surface of metal NPs and NH_2-functionalized small organic molecules, offering substantial advantages for host electrode performance.[122–126] Consequently, this unique approach can provide a significant basis for developing robust and efficient enzymatic bioelectrodes for various biotechnological applications, including EBFCs. EBFCs. In Section 3, we will present the high-performance EBFCs developed using this LER-LbL assembly, showcasing their high power output and operational stability.

3. High-performance EBFCs

3.1. EBFCs Using Hydrophilic GOx/Hydrophobic Au NP Multilayers and Cotton Fibers

Recently, for developing high-performance EBFCs, a LER-LbL assembly has been applied to the fabrication of conductive cotton fibers with an extremely large surface area as well as the conductive linkers bridging between adjacent GOx. First, this transformation from insulating cotton fibers to conductive cotton fibers can be confirmed by Fourier transform infrared (FTIR) spectroscopy, which tracks the consecutive appearance and disappearance of the ligand peak.[50,127] Moreover, the application of these assembly techniques can be extended beyond the host electrode to the electrochemically active layers that form the anode and cathode.

As a pioneering work, Kwon et al. developed a high-performance EBFC by utilizing densely packed Au NP-coated cotton fiber as the host electrode.[128] To achieve this, tetra(octylammonium bromide)-stabilized Au NPs (TOABr-Au NPs) in toluene were densely deposited on insulating cotton fibers via an unconventional LER-LbL assembly. Instead of employing bulky/insulating polymer linkers, they utilized tris(2-aminoethyl)amine (TREN) molecular linkers with amine (NH_2)

© 2024 The Author(s). Advanced Functional Materials published by Wiley-VCH GmbH

16163028, 2025, 16, Downloaded from https://advanced.onlinelibrary.wiley.com/doi/10.1002/adfm.202415933 by Korea University Library, Wiley Online Library on [20/09/2026]. See the Terms and Conditions (https://onlinelibrary.wiley.com/terms-and-conditions) on Wiley Online Library for rules of use; OA articles are governed by the applicable Creative Commons License

groups in ethanol (**Figure 6a**). These NH_2 groups of the TREN linkers exhibited a strong affinity for the bare surface of Au NPs, facilitating an in situ ligand exchange reaction between the bulky TOABr ligands bound to the surface of Au NPs and the TREN linkers during LbL deposition. The assembly process was repeated until reaching the desired bilayer number (n) of $(TOABr\text{-}Au\ NP/TREN)_n$ multilayers, as confirmed by FTIR analysis (Figure 6b). This approach notably reduced the separation distance between vertically adjacent Au NPs, thereby enhancing the electrical conductivity of the $(TOABr\text{-}Au\ NP/TREN)_n$-coated cotton fiber. The resulting cotton electrode demonstrated exceptional electrical conductivity ($\approx 2.1 \times 10^4$ S cm^{-1}), extremely low R_s and R_{ct} values of 30 and 4 Ω, mechanical flexibility, and a large surface area per unit area, which served as both an enzyme reservoir and a conductive host electrode (Figure 6c,d).

A further modification of this host electrode involved electrostatic LbL assembly between negatively charged GOx enzymes and positively charged TREN in a PBS solution to create the anode of the DET-EBFC. Particularly, the use of TREN molecular linkers could minimize the separation distance between adjacent GOx layers as well as between adjacent Au NPs. In addition, the cotton host electrode, when coated with Au NPs to facilitate high ORR, could also serve as the cathode. The resulting complete cell device, consisting of cotton host electrode-based anode (i.e., $(GOx/TREN)_{30}/(TOABr\text{-}Au\ NP/TREN)_{20}$-coated cotton fiber) and cathode (i.e., $(TOABr\text{-}Au\ NP/TREN)_{120}$-coated cotton fiber), demonstrated a maximum areal power density of 3.7 mW cm^{-2} (at 300 mmol L^{-1} glucose concentration) and excellent operational stability, retaining ≈79% and 62% of its initial OCV and power density, respectively, after 35 days in a 10 mmol L^{-1} glucose buffer (Figure 6e–g). In this case, optimal EBFC performance was achieved at a glucose concentration condition of 300 mmol L^{-1}, which is significantly higher than the physiological glucose concentration ranging from ≈5 to 10 mmol L^{-1} found in the body.[129] Evaluation of performance at low glucose concentrations is crucial for devices intended for internal use, such as implants, where practical applicability is essential. Conversely, performance at higher concentrations is relevant for external biomedical devices. Therefore, evaluation of EBFC performance under both high and low concentration conditions is essential, as it provides valuable insight into the potential applications of these devices. As a result, a balanced assessment is required to determine their suitability for various biomedical applications.

3.2. EBFCs Using Hydrophilic Gox/Hydrophobic ITO NP Multilayers and Multiplied Structure

More recently, Cho and co-workers reported a more advanced hybrid EBFC using a novel amphiphilic LbL assembly. This innovation addresses the challenge posed by the stark difference in solvent polarity between hydrophilic GOx in water and hydrophobic TOABr-Au NPs in toluene, as a kind of the LER-LbL assembly mentioned above (**Figure 7a**).[130] In particular, a key aspect of this approach is the ability to directly deposit amino acid groups of GOx onto the bare surface of TOABr-Au NPs. This process triggers a ligand exchange reaction between the pristine TOABr ligands, loosely bound to the surface of Au NPs, and the amino acid groups (specifically amine groups) of GOx. Furthermore, the amphiphilic assembly approach is characterized by the fact that the conductive Au NP linkers, which directly bridge the interfaces between adjacent GOx layers, can significantly enhance the electron transfer between adjacent GOx layers as well as between the host electrode and the GOx layer (Figure 7b). In the case of using the $(TOABr\text{-}Au\ NP/TREN)_n$-coated cotton fiber as the host electrode, the complete cell DET-EBFC composed of the $(GOx/Au\ NP)_n/(TOABr\text{-}Au\ NP/TREN)_n$-coated cotton fiber (for the anode) and the Pt-sputtered $(Au\ NP/TREN)_n$-coated cotton fiber (for the cathode) exhibited a remarkably high power density of 7.3 mW cm^{-2} and high operational stability (Figure 7c). The stability of this assembly was tested during continuous operation in PBS solution containing 10 mmol L^{-1} glucose for 60 days, maintaining ≈61% of the initial power density (Figure 7d). These results demonstrate that the formation of stable covalent bonds between the amine groups of GOx and the surface of the Au NPs, as well as between the host electrode and GOx, significantly contributed to the robust immobilization of GOx.

Very recently, the Cho group presented a powerful hybrid EBFC using conductive ITO NPs with pointed axes, specifically bipod and/or tripod type oleylamine (OAm)-stabilized ITO NPs (OAm-ITO NPs) (**Figure 8a**).[64] These axes mimic the structure of redox mediators with long-space arms that increase the contact possibilities between the mediators and the active sites (FAD) of GOx. An additional advantage of this approach lies in the robust covalent bonding-based LbL assembly, which can significantly improve the electron transfer and operational stability of the GOx-based electrode. This improvement is achieved by increasing the packing density and robust immobilization of hydrophobic OAm-ITO NPs without long-range electrostatic repulsion between the same OAm-ITO NPs on the hydrophilic GOx layer. This favorable interfacial interaction relies on a ligand exchange reaction facilitated by multiple affinities between the bare surface of ITO NPs and the amino acid groups within GOx. Therefore, during LbL deposition, these amino acid groups replace loosely bound hydrophobic OAm ligands, similar to the adsorption behavior observed in the LER-LbL assembly between TOABr-Au NPs and GOx. The anode fabricated by the above methods exhibited an outstanding k_s value of 6.3 ± 0.1 s^{-1} (Figure 8b,c), demonstrating that the ITO NPs effectively enhanced the electron transfer from GOx to the host electrode. Incorporating these combined approaches, the complete cell device composed of the $(GOx/ITO\ NP)_n/(Au\ NP/TREN)_n$-coated cotton fiber (for the anode) and the Pt-sputtered $(Au\ NP/TREN)_n$-coated cotton fiber (for the cathode) achieved a high maximum power density of 4.7 mW cm^{-2} at 300 mmol L^{-1} glucose concentration and 2.0 mW cm^{-2} at 10 mmol L^{-1} glucose concentration (Figure 8d,e). Furthermore, a multi-ply structured fiber system, which increases the active surface area without proportionally enlarging the electrode, raised the maximum power density of the complete cell EBFC from 4.7 to 10.4 mW cm^{-2} at the same glucose concentration (Figure 8f,g). This multi-ply EBFC was also able to maintain ≈49% (corresponding to 2.1 mW cm^{-2}) of the initial power density at 10 mmol L^{-1} glucose even after 60 days (Figure 8h).

As a result, 1) favorable interfacial interaction using small molecule linker- and/or LER-LbL assemblies LbL assemblies, 2) effective electron transfer using densely packed conductive linkers, and 3) effective structural design using highly porous

© 2024 The Author(s). Advanced Functional Materials published by Wiley-VCH GmbH

16163028, 2025, 16, Downloaded from https://advanced.onlinelibrary.wiley.com/doi/10.1002/adfm.202415933 by Korea University Library, Wiley Online Library on [20/09/2026]. See the Terms and Conditions (https://onlinelibrary.wiley.com/terms-and-conditions) on Wiley Online Library for rules of use; OA articles are governed by the applicable Creative Commons License

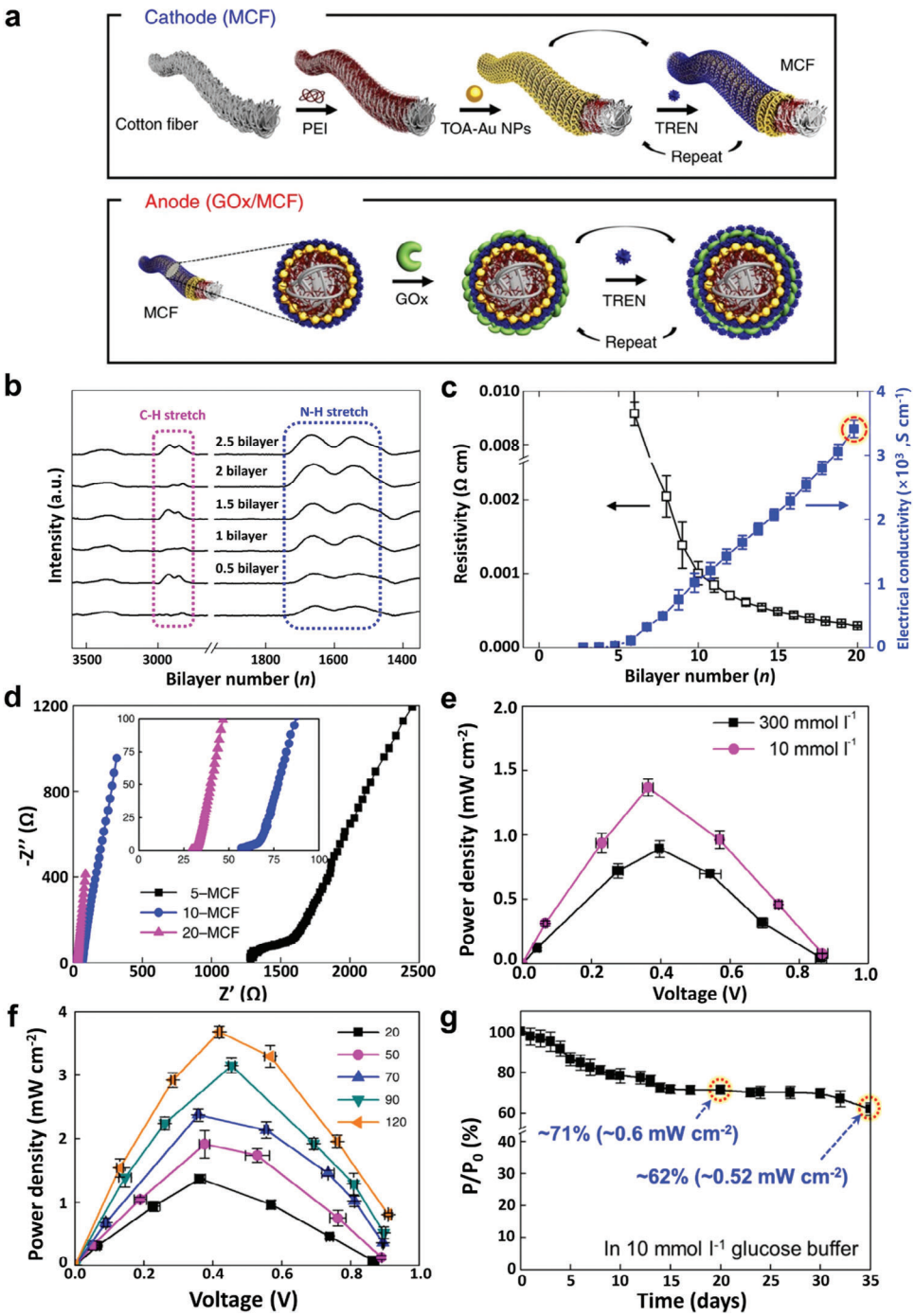

Figure 6. Au NP-coated fiber-based hybrid EBFCs. a) Illustration of the preparation of the metallic cotton fiber (MCF)-based cathode and the GOx/MCF-based anode using small-molecule ligand-induced layer-by-layer assembly. In the first step, bare cotton fiber was coated with poly(ethylenimine) (PEI, M_w ~800). Characterization of the metallic cotton fiber electrode. Reproduced with permission.[128] Copyright 2018, Springer Nature. b) FTIR spectra of the (TOA-Au NP/TREN)$_n$ multilayers as a function of n. Reproduced with permission.[128] Copyright 2018, Springer Nature. c) Resistivity and electrical conductivity of n-MCFs as a function of n. The error bars show the standard deviation from the mean value of the electrical conductivities for 3–5 independent experiments. Reproduced with permission.[128] Copyright 2018, Springer Nature. d) Nyquist plots of n-MCFs in the frequency range 0.2 Hz to 100 kHz. Inset: Nyquist plots magnified in the high-frequency range. The equivalent series resistance (ESR) values of $n = 5$, 10, and 20 were 1346, 60, and 30 Ω, respectively. Reproduced with permission.[128] Copyright 2018, Springer Nature. e) Power output of the complete BFC consisting of the 30-GOx/20-MCF anode and 20-MCF cathode as a function of voltage. Reproduced with permission.[128] Copyright 2018, Springer Nature. f) Power output of the MCF-BFCs (an n-MCF cathode and 30-bilayered GOx/TREN multilayer-coated 20-bilayered MCF anode) with external resistors (1 kΩ–10 MΩ) as a function of n-MCF. Reproduced with permission.[128] Copyright 2018, Springer Nature. g) Relative power retention (P/P_0) of the complete MCF-BFC in 10 mmol L^{-1} glucose buffer for 35 days. The changes in the power output changes of MCF-BFCs with external resistors were continuously measured as a function of time. The error bars show the standard deviation from the mean value of the power densities for three to five independent experiments. Reproduced with.[128] Copyright 2018, Springer Nature.

© 2024 The Author(s). Advanced Functional Materials published by Wiley-VCH GmbH

16163028, 2025, 16, Downloaded from https://advanced.onlinelibrary.wiley.com/doi/10.1002/adfm.202415933 by Korea University Library, Wiley Online Library on [20/09/2026]. See the Terms and Conditions (https://onlinelibrary.wiley.com/terms-and-conditions) on Wiley Online Library for rules of use; OA articles are governed by the applicable Creative Commons License

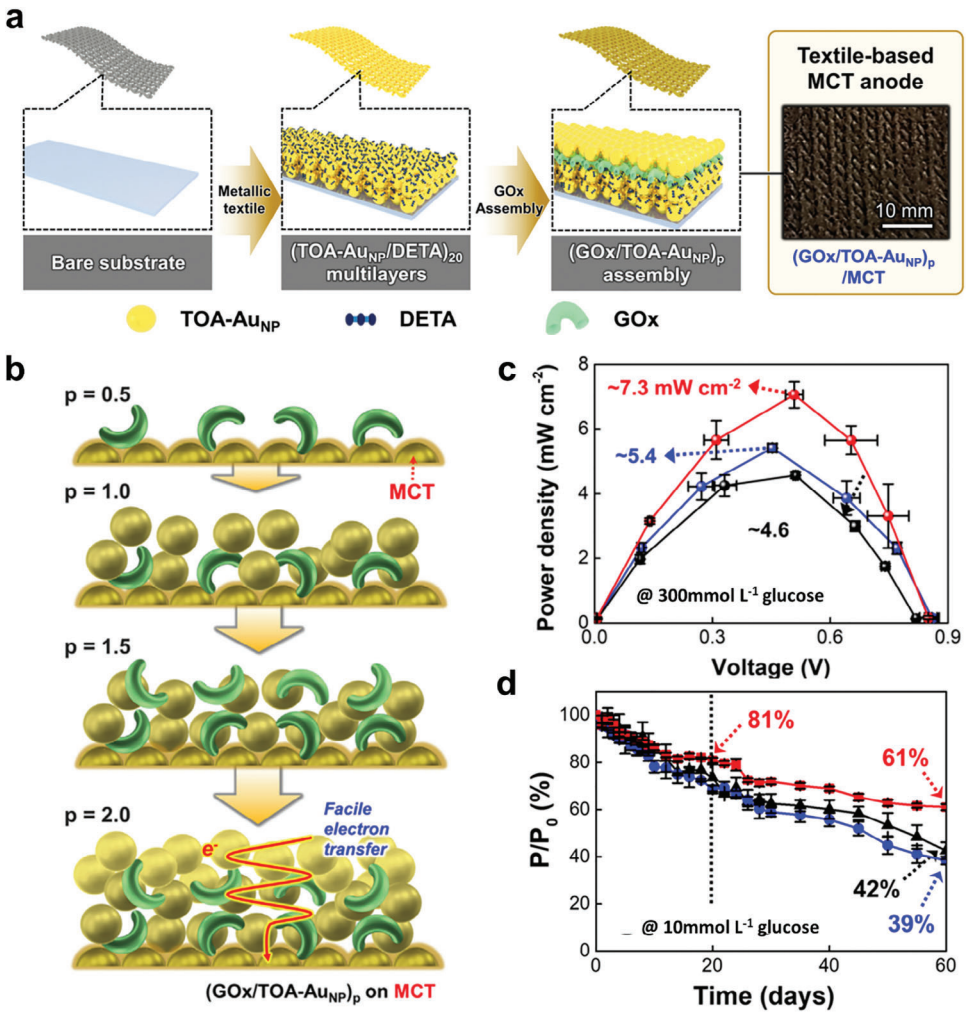

Figure 7. Amphiphilic Assembly of Au NP/GOx for hybrid EBFCs. a) Schematic (left) and optical image (right) of the (GOx/TOA-Au NP)$_n$-assembled metallic cotton textile (MCT) anode. Reproduced with permission.[130] Copyright 2022, AIP Publishing. b) Schematic illustration of the subsequent deposition of (GOx/TOA-Au NP)$_n$ multilayers on MCT, which significantly enhances the electron transfer between adjacent GOx layers as well as between GOx layer and MCT. Reproduced with permission.[130] Copyright 2022, AIP Publishing. c) Power (P)-voltage (V) profiles of single MCF-BFCs with the (GOx/TOA-Au NP)$_3$/MCF//Pt-20-MCF (black), (GOx/TOA-Au NP/DETA/TOA-Au NP)$_3$/MCF//Pt-100-MCF (red). The power output was obtained in PBS solution containing 300 mmol L^{-1} glucose (under ambient conditions at 36.5 °C) by measuring the current flowing through external variable resistors (from 1 kΩ to 10 GΩ) to control the cell potential. Reproduced with permission.[130] Copyright 2022, AIP Publishing. d) Relative power retention (P/P$_0$) of the complete BFCs with three different anodes in 10 mmol L^{-1} glucose in PBS over 60 days. Reproduced with permission.[130] Copyright 2022, AIP Publishing.

and conductive host electrodes can significantly enhance the electron transfer within the electrode and the operational stability (**Figure 9**). Furthermore, the power output and stability of glucose-based EBFCs reported to date are compared in terms of enzyme immobilization techniques, enzyme loading, and active surface area (**Table 2**). These methodologies can serve as a foundational framework for developing high-performance biomedical devices that require EBFCs as biocompatible power sources.

4. Integration of EBFCs into Biomedical Devices

Beyond efforts to improve the power performance and operational stability of EBFCs, significant research has focused on integrating EBFCs with various biomedical devices. These integrations include applications in wearable and implantable power supplies, bio-signal monitoring systems, and drug delivery systems.[134–136] Incorporating EBFCs into biomedical devices is crucial, as it enables sustainable, self-contained power sources that improve the functionality and autonomy of medical devices. This is particularly important for devices that need to operate continuously within the human body or in remote settings where frequent battery replacements are impractical. Additionally, this research extends to the development of related devices for biomedical applications, further broadening the potential impact of EBFCs in healthcare.

For example, Bi and co-workers developed a self-powered biosensing system based on an EBFC utilizing hierarchical porous metal–organic frameworks (MOFs) to enhance enzyme

© 2024 The Author(s). Advanced Functional Materials published by Wiley-VCH GmbH

16163028, 2025, 16, Downloaded from https://advanced.onlinelibrary.wiley.com/doi/10.1002/adfm.202415933 by Korea University Library, Wiley Online Library on [20/09/2026]. See the Terms and Conditions (https://onlinelibrary.wiley.com/terms-and-conditions) on Wiley Online Library for rules of use; OA articles are governed by the applicable Creative Commons License

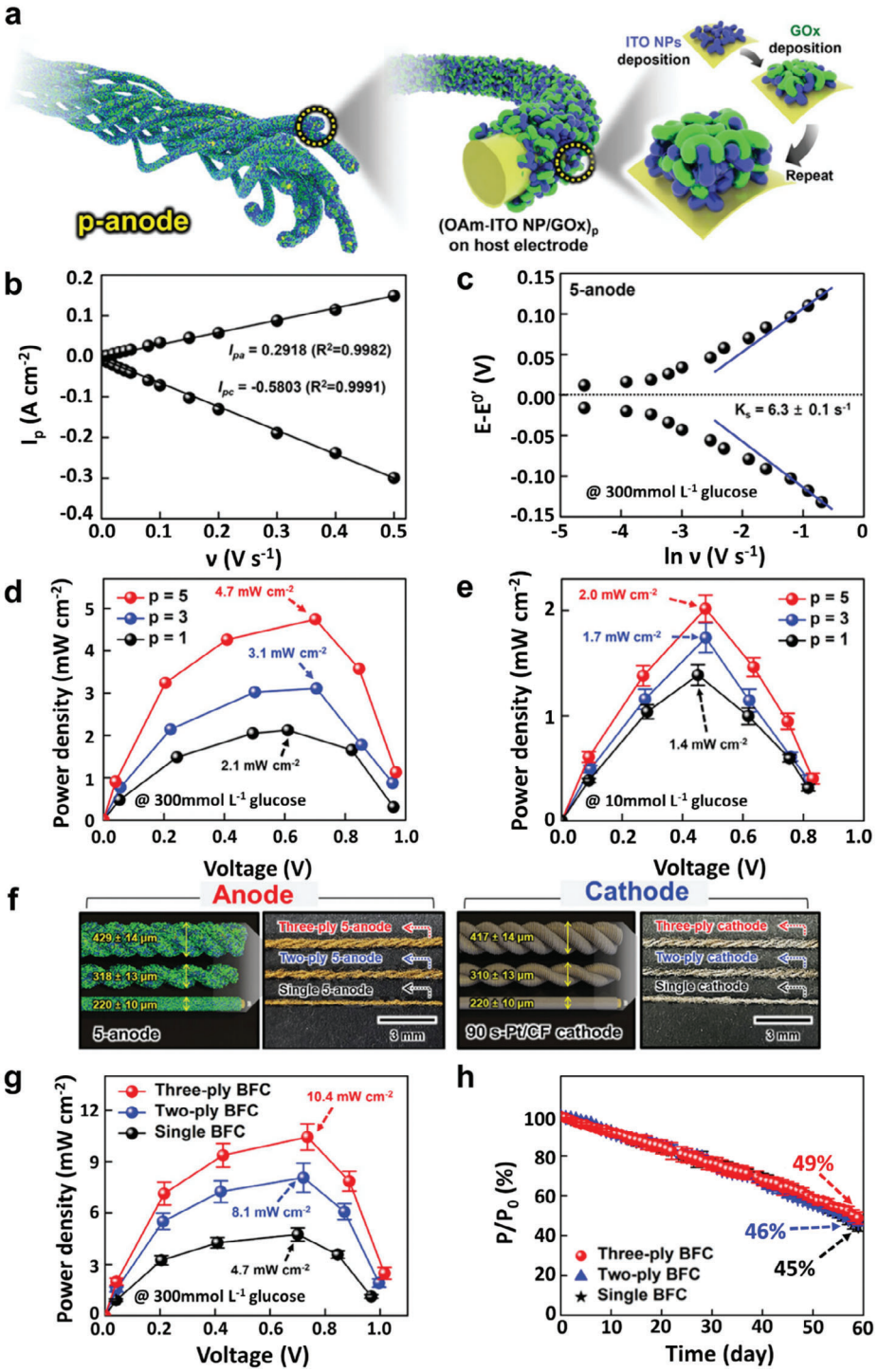

Figure 8. Amphiphilic assembly of ITO NP/GOx for hybrid EBFCs. a) Schematic illustration of p-anode Reproduced with permission.[64] Copyright 2023, Wiley-VCH. b) Change in the peak current of the 5-anode with increasing scan rate (v) from 0.005 to 0.5 V s^{-1} in PBS solution containing 300 mmol L^{-1} glucose at 36.5 °C. Reproduced with permission.[64] Copyright 2023, Wiley-VCH. c) Change in the potential ($E-E^0$) of 5-anode as a function of ln v at a 300 mmol L^{-1} glucose. Reproduced with permission.[64] Copyright 2023, Wiley-VCH. d) Power output of the complete BFCs as a function of bilayers number (p) in PBS solution containing 300 mmol L^{-1} glucose at 36.5 °C. Reproduced with permission.[64] Copyright 2023, Wiley-VCH. e) Power output of the complete BFCs as a function of the bilayer number (p) in PBS solution containing 10 mmol L^{-1} glucose at 36.5 °C. Reproduced with permission.[64] Copyright 2023, Wiley-VCH. f) Schematic illustration and photographic images of multi-ply anode and cathode. Reproduced with permission.[64] Copyright 2023, Wiley-VCH. g) Power output of the complete BFCs as a function of bilayers number (p) in PBS solution containing 300 mmol L^{-1} glucose at 36.5 °C. Reproduced with permission.[64] Copyright 2023, Wiley-VCH. h) Relative power retention (P/P_0) of the complete BFCs of multi-ply electrodes in PBS solution containing 10 mmol L^{-1} glucose at 36.5 °C. Reproduced with permission.[64] Copyright 2023, Wiley-VCH.

 © 2024 The Author(s). Advanced Functional Materials published by Wiley-VCH GmbH

16163028, 2025, 16, Downloaded from https://advanced.onlinelibrary.wiley.com/doi/10.1002/adfm.202415933 by Korea University Library, Wiley Online Library on [20/09/2026]. See the Terms and Conditions (https://onlinelibrary.wiley.com/terms-and-conditions) on Wiley Online Library for rules of use; OA articles are governed by the applicable Creative Commons License

Table 2. Electrochemical performance comparison of EBFCs using glucose fuel.

Anode	Cathode	Immobilization method	Enzyme loading amount	Electroactive area	Maximum power density [mW cm^{-2}]	Stability [period]	Refs.
NAD-GDH/VK_3/CF[a)]-Ti mesh	BOD/$Fe(CN)_6^{4-/3-}$/CF-Ti mesh	Adsorption	–	20.4 cm^2	1.45	–	[131]
PVP-[Os(*N*,*N*′-alkylanated-2,2′bi-imidazole)$_3$]$^{2+/3}$/GOx-CNT	PAA-PVI-[Os(4,4′-dichloro-2,2′-bipyridine)$_2$Cl]$^{+/2+}$/BOD-CNT	Cross–linking	226 µg	300 m^2 g^{-1}	0.74	82% (8 h)	[80]
GOx/Catalase/MWCNT	Lac/MWCNT	Entrapment/ Adsorption	–	52 cm^2	1.3	96% (30 days, 4 °C storage)	[99]
GOx/PVI-[Os(4,4′-dimethoxy-2,2′-bipyridine)$_2$Cl]$^{+/2+}$-CNT	BOD/PAA-PVI-Os(4,4′-dichloro-2,2′-bipyridine)$_2$]$^{+/2+}$-CNT	Cross–linking	25 µg, anode 13 µg, cathode	0.75 mm^2	2.18	83% (24 h)	[48]
Graphene/Au NP/GOx	Graphene/Au NP/Lac	Covalent bonding	–	–	1.96	66% (70 days)	[29]
Au/PANI[b)]/GOx	Au/PANI/Lac	Cross–linking	–	0.16 cm^2	0.69	79% (30 days)	[132]
FAD-GDH/ Os(dmb)$_2$PVI[c)]/ EPD[d)]-MWCNTs/GCE[e)]	Lac/Os(bpy)$_2$PVI/ EPD-MWCNTs/GCE	Covalent bonding	–	–	0.43	56% (7days)	[25]
[(TPA[f)]/HRP/GOx)]/PEI/CNT	Pt/C-Nafion 117	Cross–linking	3.71 mg, anode	0.25 cm^2	2.1	85.8% (20 days)	[95]
(GOx/TREN)$_{30}$-MCF	MCF	Covalent bonding	–	3.1 mm^2	3.7	71% (20 days)	[128]
$NiMoSe_2$/GOx/Nickel foam	$NiMoSe_2$/Lac/Nickl foam	Entrapment	–	24 m^2 g^{-1}	1.2	89.5% (3 days)	[133]
FAD-GDH/poly(GMA)-modified AmFc	BOD/2,2′azino-bis(3-ethylbenzothiazoline-6-sulfonic acid)	Cross–linking	–	25 mm^2	3.6	–	[82]
CNT/PDA[g)]/GOx/PEI/Nafion	Pt/C	Cross–linking	–	–	0.55	72% (21 days)	[85]
Au NP/LIG/GOx-PLGA[h)]	Au NP/LIG/Lac-PLGA	Adsorption	5 (U)	–	0.48	33.9% (7 days)	[96]
(GOx/Au NP)$_n$-MCT	Pt-(Au NP/DETA)$_n$-MCT	Covalent bonding	6.9 µg, anode	3.1 mm^2	7.3	81% (20 days)	[130]
(GOx/ITO NP)$_n$/(Au NP/TREN)$_n$-cotton fiber	Pt-(Au NP/TREN)$_n$ -cotton fiber	Covalent bonding	–	6.28 mm^2	10.4	49% (60 days)	[64]
(Os-RM[i)]/GOx/Os-RM/TOA-Au NP)$_3$.CCF	Pt-CCF	Covalent bonding	–	6.28 mm^2	8.5	47% (30 days)	[15]

[a)] CF: carbon fiber; [b)] PANI: polyaniline; [c)] Os(dmb)$_2$PVI: [Os(4,4′-dimethyl-2,2′-bipyridine)$_2$(poly-vinylimidazole)$_{10}$Cl]$^+$; [d)] EPD: Electrophoretic deposition; [e)] GCE: glassy carbon electrode; [f)] TPA: terephthalaldehyde; [g)] PDA: polydopamine; [h)] PLGA: poly(lactic-*co*-glycolic acid); [i)] RM: redox mediator.

© 2024 The Author(s). Advanced Functional Materials published by Wiley-VCH GmbH

16163028, 2025, 16, Downloaded from https://advanced.onlinelibrary.wiley.com/doi/10.1002/adfm.202415933 by Korea University Library, Wiley Online Library on [20/09/2026]. See the Terms and Conditions (https://onlinelibrary.wiley.com/terms-and-conditions) on Wiley Online Library for rules of use; OA articles are governed by the applicable Creative Commons License

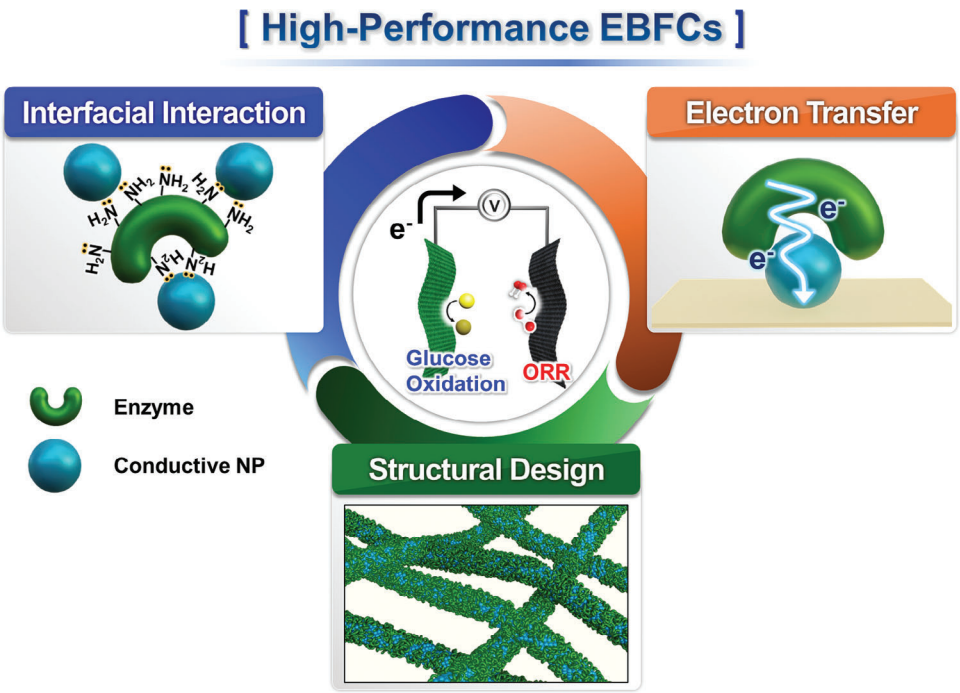

Figure 9. Schematic illustration of high-performance EBFCs using LER-LbL assembly.

stability and reactivity (**Figure 10a**).[134] By encapsulating enzymes within a high-surface-area MOF structure, catalytic activity was significantly boosted. The porous MOF, synthesized with tannic acid (TA) for structural etching, co-encapsulated the Field-emission and the nicotinamide adenine dinucleotide (NAD^+) cofactor in a zeolitic imidazolate framework (ZIF-L), forming the composite GDH/NAD^+@ZIF-L@TA (Figure 10b). This configuration optimized substrate-enzyme interactions, leading to efficient catalytic reactions. This EBFC-based system generated electricity through enzyme-driven transfer, enabling the detection of biomolecules such as microRNAs (miRNA) without the need for external power. This self-sufficient approach is advantageous for analyzing real biological samples. Additionally, the system incorporated cascade signal amplification, which increased detection sensitivity and enabled the effective detection of miRNA at low concentrations (Figure 10c). This system demonstrated a maximum power density of 239.23 μW cm^{-2} and maintained over 74% of its power response after five days of operation (Figure 10d). The proposed biosensor effectively detected miRNA-21 through target-triggered dual amplification mediated by a DNA tetrahedron, making it valuable for early diagnosis and treatment monitoring. This study demonstrated an innovative biosensor technology using hierarchical porous MOFs, which maximized enzyme stability and reactivity while enhancing the sensing sensitivity for efficient biomolecule detection.

In another recent research, Maity et al. developed a metabolic fuel cell that utilizes blood sugar as fuel, exploring the potential for a self-sufficient bio-electronic device.[135] This innovative fuel cell system efficiently converted blood sugar into electrical energy, representing a significant advance in continuous health monitoring and treatment by self-powered bio-electronic devices (**Figure 11a**). The EBFC was constructed with a nanocomposite anode composed of cupric oxide (CuO) NPs, MWCNTs, and poly(3,4-ethylenedioxythiophene):poly(styrene sulfonate) (PEDOT:PSS) immobilized on graphite felt and a nanocomposite cathode made of Nafion-coated carbon black containing Pt NPs (Figure 11b). The power density and output voltage of the metabolic fuel cell were measured at various blood sugar concentrations, showing how the power density and OCV were changed with increasing blood sugar levels (Figure 11c,d). The cell achieved a maximum power density of 0.7 mW cm^{-2} and an OCV of ≈0.9 V at a glucose concentration of 50 mmol L^{-1}. Furthermore, the study assessed the impact of the metabolic fuel cell on the human body by measuring indicators such as cell viability and inflammatory response, demonstrating its potential for practical application in biomedical devices and underscoring its relevance in the field.

The long-standing goals of EBFCs are to power implantable medical devices and on-body biosensors, particularly when integrated into various biomedical systems. Enhancements in power performance, stability, flexibility, and miniaturization, create opportunities to combine EBFCs with emerging technologies. The integration of EBFCs with flexible electronics and wireless communication systems could lead to revolutionary applications previously deemed inconceivable.[137–139] This synergy may enable the development of fully integrated, self-powered biomedical devices capable of real-time monitoring and data transmission. Such innovations have the potential to transform patient care by providing continuous health monitoring and personalized treatment, especially in remote settings where conventional power sources are impractical. Although the integration of EBFCs into biomedical devices is still in its early stages, the progress made thus far is promising. For example, Zhu's group reported that a compact drug delivery model with self-diagnosis

© 2024 The Author(s). Advanced Functional Materials published by Wiley-VCH GmbH

16163028, 2025, 16, Downloaded from https://advanced.onlinelibrary.wiley.com/doi/10.1002/adfm.202415933 by Korea University Library, Wiley Online Library on [20/09/2026]. See the Terms and Conditions (https://onlinelibrary.wiley.com/terms-and-conditions) on Wiley Online Library for rules of use; OA articles are governed by the applicable Creative Commons License

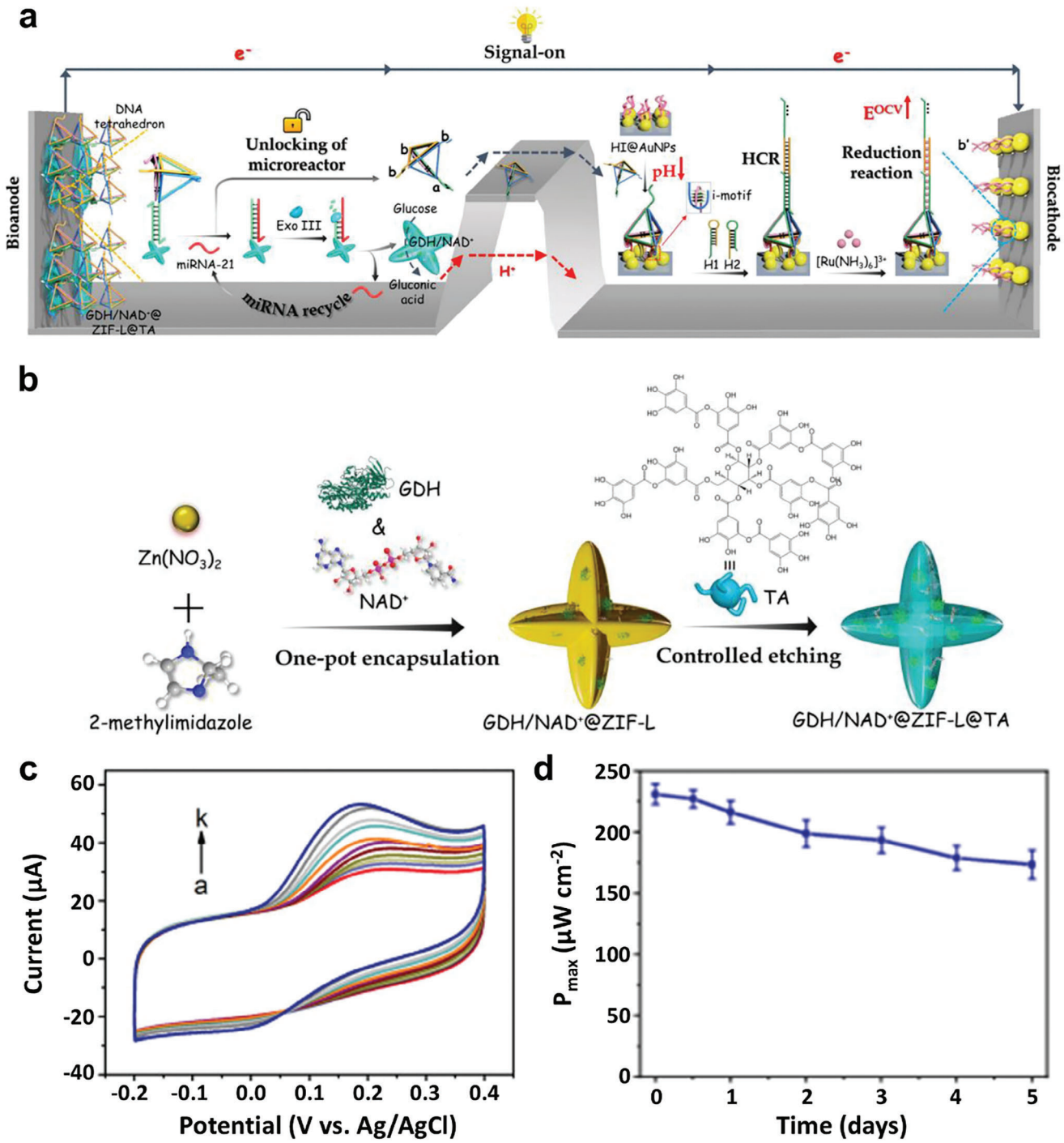

Figure 10. Hierarchical porous MOF-based EBFCs. a) Schematic illustration of a membrane-less BFC-based self-powered biosensor for the "signal-on" detection of miRNA-21 based on biocatalytic MOF microreactor and DNA tetrahedron-mediated two-step cascade amplification strategy. Reproduced with permission.[134] Copyright 2023, Wiley-VCH. b) Schematic illustration of the synthesis of hierarchical porous ZIF-L-based microreactor by controlled-etching strategy. Reproduced with permission.[134] Copyright 2023, Wiley-VCH. c) CV of GDH/NAD$^+$@ ZIF-L@TA microreactor-modified fluorine-doped tin oxide (FTO) bioanode in response to glucose at different concentrations (from a to k: 0 to 10 mmol L^{-1} at 1 mmol L^{-1} intervals). The scanning rate is 50 mV s^{-1}. Reproduced with permission.[134] Copyright 2023, Wiley-VCH. d) P_{max} responses of EBFC operated over a period of five days. Reproduced with permission.[134] Copyright 2023, Wiley-VCH.

 © 2024 The Author(s). Advanced Functional Materials published by Wiley-VCH GmbH

16163028, 2025, 16, Downloaded from https://advanced.onlinelibrary.wiley.com/doi/10.1002/adfm.202415933 by Korea University Library, Wiley Online Library on [20/09/2026]. See the Terms and Conditions (https://onlinelibrary.wiley.com/terms-and-conditions) on Wiley Online Library for rules of use; OA articles are governed by the applicable Creative Commons License

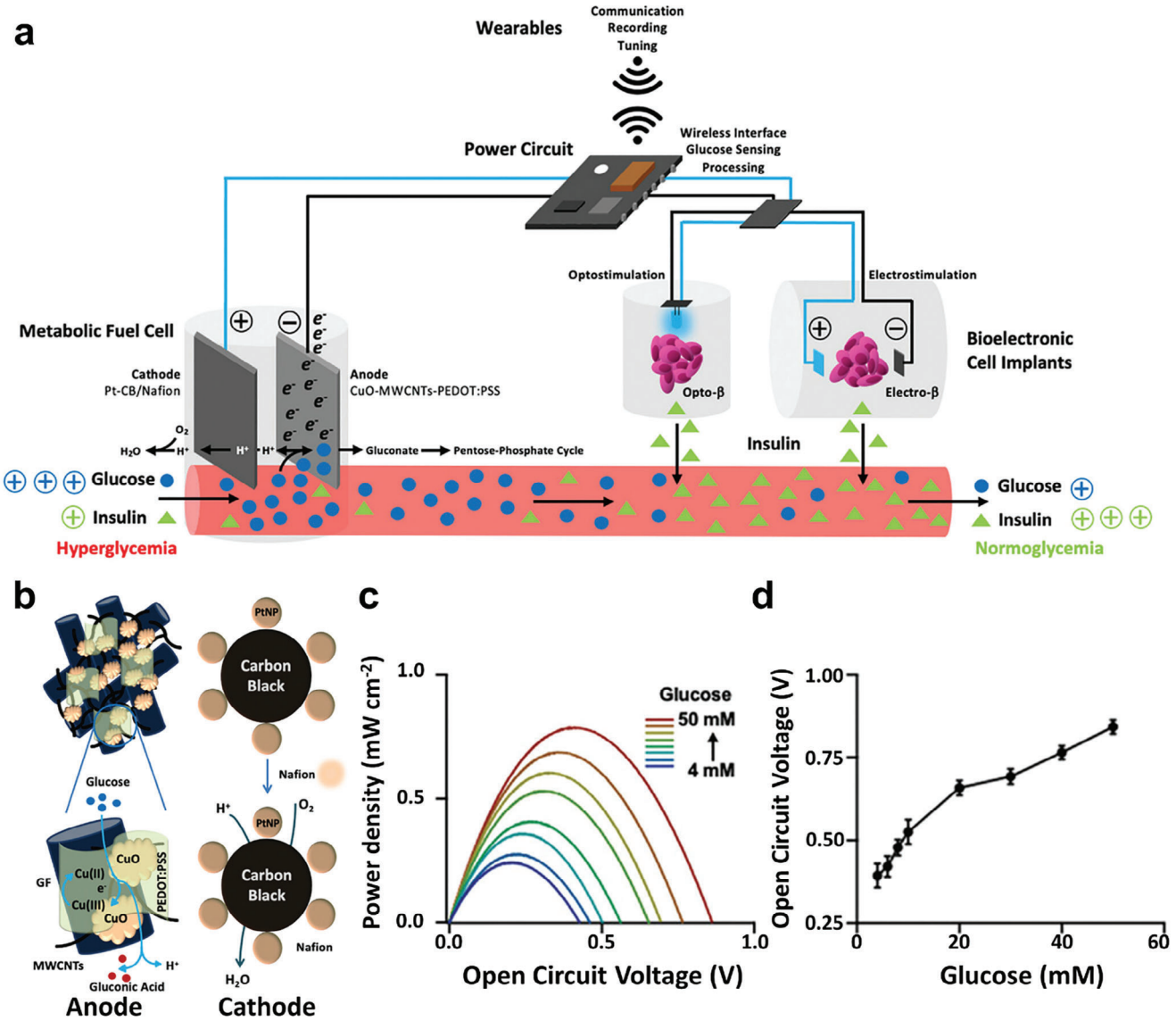

Figure 11. Self-sufficient EBFC-based bio-electronic device. a) Schematic of the non-enzymatic metabolic fuel cell for closed-loop control of blood-glucose homeostasis. Operation of the metabolic fuel cell. After implantation, the metabolic fuel cell is connected to the bloodstream. The electrons travel to the power circuit which provides a wireless interface with the wearables for communication, recording, and tuning, manages the glucose sensing, and processes the operation of the metabolic fuel cell at blood-glucose levels above 10 mmol L^{-1} glucose. The harnessed electrical energy is used to stimulate engineered human cells to release therapeutic proteins such as insulin in response to light (optostimulation of Opto-β cells) or electric fields (electrostimulation of Electro-β cells). Reproduced with permission.[135] Copyright 2023, Wiley-VCH. b) Schematic of the nanocomposite anode material consisting of cupric oxide (CuO) nanoparticles, MWCNTs, and PEDOT:PSS immobilized on a graphite felt (left). Schematic of the nanocomposite cathode material consisting of Nafion-coated carbon black (CB)-containing Pt NP (right). Characterization and performance analysis of the metabolic fuel cell. Reproduced with permission.[135] Copyright 2023, Wiley-VCH. c) Power density, d) OCV for different glucose concentrations. Reproduced with permission.[135] Copyright 2023, Wiley-VCH.

and self-evaluation could be developed by integration of a targeted drug delivery system with a robust glucose/O_2 EBFC-based self-powered biosensor.[140] By employing a comprehensive design that encompasses diagnostic even-triggered drug delivery on the anode, competitive reaction, blocking effect, and the establishment of an evaluation model on the cathode, they successfully fabricated an in vitro integrated platform. They also demonstrated that the stability and output performances of the EBFC-based self-powered biosensors were sufficient to enable long-term dynamic evaluation, as well as highly sensitive diagnosis and evaluation within an in vitro integrated platform. Chung group also reported an animal brain stimulator that incorporates a power management integrated circuit to harvest energy from EBFCs. In this setup, EBFC can supply 28.4 mJ to the ABS over 10 min, enabling the resulting EBFC-ABS system to be implanted in flying birds.[141]

Continued interdisciplinary collaboration among bioengineering, materials science, and medical research will be crucial to

© 2024 The Author(s). Advanced Functional Materials published by Wiley-VCH GmbH

16163028, 2025, 16, Downloaded from https://advanced.onlinelibrary.wiley.com/doi/10.1002/adfm.202415933 by Korea University Library, Wiley Online Library on [20/09/2026]. See the Terms and Conditions (https://onlinelibrary.wiley.com/terms-and-conditions) on Wiley Online Library for rules of use; OA articles are governed by the applicable Creative Commons License

overcoming current challenges and unlocking the full potential of EBFCs in biomedical applications. As research progresses, the vision of self-powered autonomous medical devices that enhance patient care and health outcomes is becoming increasingly achievable.

5. Conclusion and Outlook

In this perspective, we have discussed the working principles, types, and electron transfer mechanisms of glucose-based EBFCs, as well as enzyme immobilization. We also introduced recent strategies for enhancing their areal power output and operational stability and explored the studies on integrating EBFCs into biomedical devices. Although glucose-based EBFCs currently lag behind commercial lithium-ion batteries, supercapacitors, and fuel cells in terms of energy performance, they hold promise as renewable, sustainable, and biocompatible power sources for compact and implantable medical devices. The slow progress has been attributed to several factors, including limitations in electrode components (such as enzymes, biocompatible host electrodes, and additives), challenges in electrode preparation and operation under physiological conditions, issues with electron transfer between enzymes and host electrodes, and difficulties with enzyme immobilization.

To overcome these fundamental limitations and enhance energy performance, employing unique structural designs and controlling interfacial interactions in the assembly of EBFC electrodes offers a promising approach, applicable to both MET- and DET-EBFCs. Key strategies discussed in this perspective include:

1) Structural design of host electrodes: Highly conductive 3D-structured host electrodes with large surface areas, such as those made of metallic fibrils, offer significant advantages over flat host electrodes. These designs increase a notable increase in enzyme loading per unit area (directly affecting areal power output) and facilitate efficient electron transfer among enzymes and between enzymes and the host electrode.
2) Incorporation of conductive components: Uniformly and densely incorporating electrically conductive components such as CNTs, conducting polymers, ITO NPs, or Au NPs into insulating enzyme layers can enhance electron transfer efficiency and significantly boost power output.
3) Interfacial interaction and enzyme immobilization: The effectiveness of enzyme immobilization and the operational stability of EBFC devices depend on the interfacial interactions between enzymes and host electrodes, as well as between adjacent enzymes. The LbL assembly method, utilizing covalently bonded enzyme/metal NP multilayer films, integrates enzyme amino acid groups with hydrophobic metal or ITO NPs on conductive host electrodes. Furthermore, this approach creates ultrathin, nanoblended structures that enhance electron transfer efficiency, power output, and operational stability. Periodic inclusion of conductive NP layers between enzyme layers acts as robust linkers and conductive elements, significantly improving enzyme immobilization and operational stability. Particularly, since the most critical issue in developing practical EBFCs is operational stability, this immobilization approach using conductive metal or metal oxide NPs can offer valuable insights for creating high-performance EBFCs.
4) Enhanced performance with LER-LbL assembly: The LbL assembly method not only improves the performance of metallic fibril-based host electrodes but also enables the creation of high-performance anode and cathode. Fibril-based EBFC electrodes (both anode and cathode) formed through controlled interfacial assembly have demonstrated exceptionally high power output exceeding 4 mW cm^{-2} and excellent operational stability, outperforming other BFC approaches.

However, despite the significant advantages of interfacial interaction-based LbL assemblies including LER-LbL assembly—such as precise control over surface chemistry and the loading of active components (e.g., enzymes, conductive components, and redox mediators)—the thin film deposition process using dip coating can be time-consuming. This is often a challenge in producing EBFC electrodes with high power performance and commercial viability. In addition, issues related to process duration and active component loading can generally be optimized by adjusting solution concentrations. More promisingly, the interfacial interaction engineering approach can be scaled up for large-scale LbL assemblies, such as automated spray deposition and roll-to-roll processes. These techniques can significantly reduce electrode fabrication time to just a few seconds per layer and enable the effective mass loading of active components onto highly porous substrates, facilitating the production of industrial-grade energy electrodes. In particular, considering that a variety of practical biomedical devices using enzyme-based electrodes have much difficulty in achieving long-term stability to several critical factors such as enzyme degradation and the detachment of enzymes from the host electrodes, the combination of ligand exchange-induced interface design of active components with advanced fabrication technology can be a breakthrough in overcoming the challenges of applying LbL assembly to practical biomedical devices using EBFC.

With this in mind, we believe that the integration of interfacial interaction-driven LbL assembly with fibril-based host electrodes holds great promise for overcoming the limitations (low power output and operational stability) of glucose-based EBFCs. Furthermore, we envision that this approach has the potential to be widely and effectively applied to other energy conversion systems beyond EBFCs.

Acknowledgements

This work was supported by a National Research Foundation of Korea (NRF) grant funded by the Korea government (Ministry of Science and ICT) (NRF-2021R1A2C3004151 and 2022R1A2C1009690). This research was also supported by the Pioneer Research Center Program through the National Research Foundation of Korea funded by the Ministry of Science, ICT & Future Planning (RS-2024-00451691).

Conflict of Interest

The authors declare no conflict of interest.

© 2024 The Author(s). Advanced Functional Materials published by Wiley-VCH GmbH

16163028, 2025, 16, Downloaded from https://advanced.onlinelibrary.wiley.com/doi/10.1002/adfm.202415933 by Korea University Library, Wiley Online Library on [20/09/2026]. See the Terms and Conditions (https://onlinelibrary.wiley.com/terms-and-conditions) on Wiley Online Library for rules of use; OA articles are governed by the applicable Creative Commons License

Author Contributions

J.P., W.C., C.H.K., and J.C. wrote and revised the manuscript. All authors discussed the results and commented on the manuscript.

Keywords

biofuel cells, conductive interfacial linkers, electron transfers, enzyme immobilization, fibril-structured host electrodes

Received: August 28, 2024
Revised: October 7, 2024
Published online: October 29, 2024

[1] S. J. Updike, G. P. Hicks, *Nature* **1967**, *214*, 986.
[2] N. Mano, F. Mao, A. Heller, *J. Am. Chem. Soc.* **2002**, *124*, 12962.
[3] F. Mao, N. Mano, A. Heller, *J. Am. Chem. Soc.* **2003**, *125*, 4951.
[4] N. Mano, F. Mao, A. Heller, *J. Electroanal. Chem.* **2005**, *574*, 347.
[5] I. Jeerapan, J. R. Sempionatto, J. Wang, *Adv. Funct. Mater.* **2019**, *30*, 1906243.
[6] X. Xiao, H. Xia, R. Wu, L. Bai, L. Yan, E. Magner, S. Cosnier, E. Lojou, Z. Zhu, A. Liu, *Chem. Rev.* **2019**, *119*, 9509.
[7] S. Hao, X. Sun, H. Zhang, J. Zhai, S. Dong, *J. Mat. Chem. B.* **2020**, *8*, 3393.
[8] A. Ruff, F. Conzuelo, W. Schuhmann, *Nat. Catal.* **2020**, *3*, 214.
[9] H. Wu, Y. Zhang, A. L. Kjøniksen, X. Zhou, X. Zhou, *Adv. Funct. Mater.* **2021**, *31*, 2103976.
[10] L. Wang, X. Wu, B. S. Q. Su, R. Song, J. Zhang, J. Zhu, *Adv. Energy Sustainability Res.* **2021**, *2*, 2100031.
[11] R. Liu, Z. L. Wang, K. Fukuda, T. Someya, *Nat. Rev. Mater.* **2022**,*7*, 870.
[12] K. Veenuttranon, K. Kaewpradub, I. Jeerapan, *Nano-Micro Lett.* **2023**, *15*, 85.
[13] S. Guan, J. Wang, Y. Yang, X. Zhu, J. Zhou, D. Ye, R. Chen, H. Dai, Q. Liao, *Adv. Funct. Mater.* **2023**, *33*, 2303134.
[14] N. Shakeel, R. Perveen, M. I. Ahamed, A. Ahmad, Inamuddin, *Fuel-Fuel* **2023**, *341*, 127579.
[15] Y. Jang, T. Seo, J. Pak, M. K. Park, J. Ahn, G. C. Jin, S. W. Lee, Y. J. Chang, Y. Choi, C. H. Kwon, J. Cho, *Adv. Energy Mater.* **2024**, *14*, 2401255.
[16] S. C. Barton, J. Gallaway, P. Atanassov, *Chem. Rev.* **2004**, *104*, 4867.
[17] Y. Yu, J. Nassar, C. Xu, J. Min, Y. Yang, A. Dai, R. Doshi, A. Huang, Y. Song, R. Gehlhar, A. D. Ames, W. Gao, *Sci. Rob.* **2020**, *5*, eaaz7946.
[18] K. Stolarczyk, J. Rogalski, R. Bilewicz, *Bioelectrochemistry* **2020**, *135*, 107574.
[19] J. A. Bauer, M. Zámocká, J. Majtán, V. Bauerová-Hlinková, *Biomolecules* **2022**, *12*, 472.
[20] J. Hernandez, J. Solla-Gullón, E. Herrero, A. Aldaz, J. M. Feliu,*J. Phys. Chem. C* **2007**, *111*, 14078.
[21] M. Liu, R. Zhang, W. Chen, *Chem. Rev.* **2014**, *114*, 5117.
[22] Y. Umasankar, R. P. Ramasamy, *ECS Trans.* **2013**, *45*, 9.
[23] M. Southcott, K. MacVittie, J. Halámek, L. Halámková, W. D. Jemison, R. Lobel, E. Katz, *Phys. Chem. Chem. Phys.* **2013**, *15*, 6278.
[24] T. Hanashi, T. Yamazaki, H. Tanaka, K. Ikebukuro, W. Tsugawa, K. Sode, *Sens. Actuators, B* **2014**, *196*, 429.
[25] Z. Zhong, L. Qian, Y. Tan, G. Wang, L. Yang, C. Hou, A. Liu, *J. Electroanal. Chem.* **2018**, *823*, 723.
[26] G. Kavaliauskaitė, P. Virbickas, G. Ziziunaite, A. Ramanavicius, A. Valiūnienė, *J. Electroanal. Chem.* **2023**, *928*, 117079.
[27] J. Lee, K. Kim, Y. Kwon, D. Khang, *Adv. Funct. Mater.* **2024**, *34*, 2309386.
[28] F. Amirouche, Y. Zhou, T. Johnson, *Microsyst. Technol.* **2009**, *15*, 647.
[29] Y. Chen, P. Gai, J. Zhang, J. Zhu, *J. Mater. Chem. A* **2015**, *3*, 11511.
[30] M. Rasmussen, S. Abdellaoui, S. D. Minteer, *Biosens. Bioelectron.* **2016**, *76*, 91.
[31] A. Nasar, R. Perveen, *Int. J. Hydrog. Energy* **2019**, *44*, 15287.
[32] P. Zhao, H. Zhang, X. Sun, S. Hao, S. Dong, *Electrochim. Acta* **2022**, *420*, 140440.
[33] Z. Kang, Y. Wang, H. Song, X. Wang, Y. P. J. Zhang, Z. Zhu, *Biosens. Bioelectron.* **2024**, *246*, 115845.
[34] M. Hoarau, S. Badieyan, E. N. G. Marsh, *Org. Biomol. Chem.* **2017**, *15*, 9539.
[35] G. A. Ellis, S. A. Diaz, I. L. Medintz, *Curr. Opin. Biotechnol.* **2021**, *71*, 77.
[36] M. H. Kabir, E. Marquez, G. Djokoto, M. Parker, T. Weinstein, W. Ghann, J. Uddin, M. M. Ali, M. M. Alam, M. Thompson, A. S. Poyraz, H. Z. Msimanga, M. M. Rahman, M. Rulison, J. Cramer, *ACS Appl. Mater. Interfaces* **2022**, *14*, 24229.
[37] Y. Degani, A. Heller, *J. Am. Chem. Soc.* **1989**, *111*, 2357.
[38] A. Heller, *J. Phys. Chem.* **1992**, *96*, 3579.
[39] S. Dutta, R. Patil, T. Dey, *Nano Energy* **2022**, *96*, 107074.
[40] J. Morshed, M. M. Hossain, A. Zebda, S. Tsujimura, *Biosens. Bioelectron.* **2023**, *230*, 115272.
[41] S. A. Ansari, Q. Husain, *Biotechnol. Adv.* **2012**, *30*, 512.
[42] J. Kim, H. Jia, P. Wang, *Biotechnol. Adv.* **2006**, *24*, 296.
[43] S. Haque, N. Duteanu, S. Ciocan, A. Nasar, Inamuddin, *J. Environ. Manage.* **2021**, *298*, 113483.
[44] S. Haque, A. Nasar, N. Duteanu, S. Pandey, Inamuddin, *Fuel* **2023**, *331*, 125634.
[45] T. d. Lumley-Woodyear, P. Rocca, J. Lindsay, Y. Dror, A. Freeman, A. Heller, *Anal. Chem.* **1995**, *67*, 1332.
[46] K. Jayakumar, R. Bennett, D. Leech, *Electrochim. Acta* **2021**, *371*, 137845.
[47] S. He, M. Lin, Q. Zheng, B. Liang, X. He, Y. Zhang, Q. Xu, H. Deng, K. Fan, W. Chen, *Adv. Healthcare Mater.* **2024**, *13*, 2303548.
[48] C. H. Kwon, S. Lee, Y. Choi, J. A. Lee, S. H. Kim, H. Kim, G. M. Spinks, G. G. Wallace, M. D. Lima, M. E. Kozlov, R. H. Baughman, S. J. Kim, *Nat. Commun.* **2014**, *5*, 3928.
[49] A. Niiyama, K. Murata, Y. Shigemori, A. Zebda, S. Tsujimura,*J. Power Sources* **2019**, *427*, 49.
[50] K. So, S. Kawai, Y. Hamano, Y. Kitazumi, O. Shirai, M. Hibi, J. Ogawa, K. Kano, *Phys. Chem. Chem. Phys.* **2014**, *16*, 4823.
[51] S. Fujita, S. Yamanoi, K. Murata, H. Mita, T. Samukawa, T. Nakagawa, H. Sakai, Y. Tokita, *Sci. Rep.* **2014**, *4*, 4937.
[52] Z. Li, Z. Kang, B. Wu, Z. Zhu, *J. Power Sources* **2021**, *506*, 230206.
[53] B. Reuillard, A. L. Goff, C. Agnès, M. Holzinger, A. Zebda, C. Gondran, K. Elouarzaki, S. Cosnier, *Phys. Chem. Chem. Phys.* **2013**, *15*, 4892.
[54] R. Hassanzadeh, R. E. Sabzi, M. Faraji, *J. Eletroanal. Chem.* **2022**, *924*,116821.
[55] H. J. Sim, D. Y. Lee, H. Kim, Y. Choi, H. Kim, R. H. Baughman, S. J. Kim, *Nano Lett.* **2018**, *18*, 5272.
[56] M. N. Zafar, I. Aslam, R. Ludwig, G. Xu, L. Gorton, *Electrochim. Acta* **2019**, *295*, 316.
[57] K. M. S. Inamuddin, S. I. Kim, I. So, S. J. Kim, *Electrochim. Acta* **2009**, *54*, 3979.
[58] A. Zebda, S. Tingry, C. Innocent, S. Cosnier, C. Forano, C. Mousty, *Electrochim. Acta* **2011**, *56*, 10378.
[59] M. Holzinger, A. L. Goff, S. Cosnier, *Electrochim. Acta* **2012**, *82*, 179.
[60] D. Wen, A. Eychmüller, *SmallSmall* **2016**, *12*, 4649.
[61] M. Bandapati, P. K. Dwivedi, B. Krishnamurthy, Y. H. Kim, G. M. Kim, S. Goel, *Int. J. Hydrog. Energy* **2017**, *42*, 27220.
[62] M. Tawalbeh, R. M. N. Javed, A. Al-Othman, F. Almomani, *FuelFuel* **2022**, *322*, 124237.
[63] E. Serag, A. El-Maghraby, A. E. Nemr, *Carbon Lett.* **2022**, *32*, 395.
[64] M. Kang, D. Nam, J. Ahn, Y. J. Chung, S. W. Lee, Y. Choi, C. H. Kwon, J. Cho, *Adv. Mater.* **2023**, *35*, 2304986.

© 2024 The Author(s). Advanced Functional Materials published by Wiley-VCH GmbH

16163028, 2025, 16, Downloaded from https://advanced.onlinelibrary.wiley.com/doi/10.1002/adfm.202415933 by Korea University Library, Wiley Online Library on [20/09/2026]. See the Terms and Conditions (https://onlinelibrary.wiley.com/terms-and-conditions) on Wiley Online Library for rules of use; OA articles are governed by the applicable Creative Commons License

[65] J. Lee, K. Hyun, J. M. Park, H. S. Park, Y. Kwon, *Int. J. Energy Res.* **2021**, *45*, 20959.
[66] Y. R. Maghraby, R. M. El-Shabasy, A. H. Ibrahim, H. M. E. Azzazy, *ACS Omega* **2023**, *8*, 5184.
[67] M. J. Moehlenbrock, S. D. Minteer, *Chem. Soc. Rev.* **2008**, *37*, 1188.
[68] J. Zhang, X. Huang, L. Zhang, Y. Si, S. Guo, H. Su, J. Liu, *Sustain. Energ. Fuels* **2020**, *4*, 68.
[69] J. H. Yang, H. R. Kim, J. H. Lee, J. Jin, H. U. Lee, S. W. Kim, *Int. J. Hydrog. Energy* **2021**, *46*, 3251.
[70] N. Mano, F. Mao, A. Heller, *J. Am. Chem. Soc.* **2003**, *125*, 6588.
[71] P. Kavanagh, D. Leech, *Phys. Chem. Chem. Phys.* **2013**, *15*, 4859.
[72] Z. Hu, Z. Kang, C. Yu, B. Wang, S. Jiao, R. Peng, *Int. J. Electrochem. Sci.* **2017**, *12*, 7103.
[73] K. Elouarzaki, D. Cheng, A. C. Fisher, J. Lee, *Nat. Energy* **2018**, *3*, 574.
[74] C. Bunte, L. Hussein, G. A. Urban, *J. Power Sources* **2014**, *247*, 579.
[75] N. P. Godman, J. L. DeLuca, S. R. McCollum, D. W. Schmidtke, D. T. Glatzhofer, *Langmuir* **2016**, *32*, 3541.
[76] M. Ammam, J. Fransaer, *J. Power Sources* **2014**, *257*, 272.
[77] M. Yuan, S. D. Minteer, *Curr. Opin. Electrochem.* **2019**, *15*, 1.
[78] I. Osadebe, P. O. Conghaile, P. Kavanagh, D. Leech, *Electrochim. Acta* **2015**, *182*, 320.
[79] A. Ruff, *Curr. Opin. Electrochem.* **2017**, *5*, 66.
[80] F. Gao, L. Viry, M. Maugey, P. Poulin, N. Mano, *Nat. Commun.* **2010**, *1*, 2.
[81] X. Xiao, K. D. McGourty, E. Magner, *J. Am. Chem. Soc.* **2020**, *142*, 11602.
[82] R. Suzuki, I. Shitanda, T. Aikawa, T. Tojo, T. Kondo, S. Tsujimura, M. Itagaki, M. Yuasa, *J. Power Sources* **2020**, *479*, 228807.
[83] G. Li, Z. Wu, C. Xu, Z. Hu, *Bioelectrochemistry* **2022**, *143*, 107983.
[84] M. Togo, A. Takamura, T. Asai, H. Kaji, M. Nishizawa, *Electrochim. Acta* **2007**, *52*, 4669.
[85] J. Ji, S. Kim, Y. Chung, Y. Kwon, *J. Ind. Eng. Chem.* **2022**, *111*, 263.
[86] S. Haque, A. N. Inamuddin, A. M. Asiri, *Chem. Phys. Lett.* **2018**, *692*, 277.
[87] S. Haque, N. Duteanu, A. Nasar, Inamuddin, *J. Power Sources* **2022**, *520*, 230867.
[88] M. Khan, Inamuddin, *Sci. Rep.* **2024**, *14*, 3324.
[89] J. H. T. Luong, J. D. Glennon, A. Gedanken, S. K. Vashist, *Microchim. Acta* **2016**, *184*, 369.
[90] P. N. Bartlett, F. A. Al-Lolage, *J. Electroanal. Chem.* **2018**, *819*, 26.
[91] Y. Liu, J. Zhang, Y. Cheng, S. P. Jiang, *ACS Omega* **2018**, *3*, 667.
[92] J. Li, Y. Liu, X. Tang, L. Xu, L. Min, Y. Xue, X. Hu, Z. Yang, *Microchim. Acta* **2020**, *187*, 80.
[93] J. Wang, *Electroanalysis* **2005**, *17*, 7.
[94] P. Bollella, I. Lee, D. Blaauw, E. Katz, *Chem. Phys.* **2020**, *21*, 120.
[95] Y. Chung, D. C. Tannia, Y. Kwon, *Chem. Eng. J.* **2018**, *334*, 1085.
[96] X. Huang, H. Li, J. Li, L. Huang, K. Yao, C. K. Yiu, Y. Liu, T. H. Wong, D. Li, M. Wu, Y. Huang, Z. Gao, J. Zhou, Y. Gao, J. Li, Y. Jiao, R. Shi, B. Zhang, B. Hu, Q. Guo, E. Song, R. Ye, X. Yu, *Nano Lett.* **2022**, *22*, 3447.
[97] N. A. Kotov, I. Dekany, J. H. Fendler, *J. Phys. Chem.* **1995**, *99*, 13065.
[98] J. Cho, K. Char, J. D. Hong, K. B. Lee, *Adv. Mater.* **2001**, *13*, 1076.
[99] A. Zebda, C. Gondran, A. L. Goff, M. Holzinger, P. Cinquin, S. Cosnier, *Nat. Commun.* **2011**, *2*, 370.
[100] J. Gonzalez, J. A. Sequí-Castellano, *Electrochim. Acta* **2021**, *365*, 137331.
[101] E. Laviron, *J. Electroanal. Chem.* **1974**, *52*, 355.
[102] E. Laviron, *J. Electroanal. Chem.* **1979**, *101*, 19.
[103] J. Huang, Y. Zhang, X. Deng, J. Li, S. Huang, H. Pang, *Chem. Eng J.* **2022**, *429*, 13214.
[104] M. Zhou, L. Deng, D. Wen, L. Shang, L. Jin, S. Dong, *Biosens. Bioelectron.* **2009**, *24*, 2904.
[105] S. Datta, L. R. Christena, Y. R. S. Rajaram, *3 Biotech* **2013**, *3*, 1.
[106] X. Yang, G. Tian, N. Jiang, B. Su, *Energy Environ. Sci.* **2012**, *5*, 5540.
[107] M. Kizling, K. Stolarczyk, P. Tammela, Z. Wang, L. Nyholm, J. Golimowski, R. Bilewicz, *Bioelectrochemistry* **2016**, *112*, 184.
[108] J. Shim, G. Y. Kim, S. H. Moon, *J. Electroanal. Chem.* **2011**, *653*, 14.
[109] C. Gonzalez-Solino, E. Bernalte, C. B. Royo, R. Bennett, D. Leech, M. D. Lorenzo, *ACS Appl. Mater. Interfaces* **2021**, *13*, 26704.
[110] R. E. Kim, S. G. Hong, S. Ha, J. Kim, *Enzyme Microb. Technol.* **2014**, *66*, 35.
[111] Y. Chung, Y. Ahn, M. Christwardana, H. Kim, Y. Kwon, *Nanoscale* **2016**, *8*, 9201.
[112] C. Schüler, F. Caruso, *Macromol. Rapid Comm.* **2000**, *21*, 750.
[113] G. Bijoy, R. Rajeev, L. Benny, S. Jose, A. Varghese, *Chemosphere* **2022**, *307*, 135759.
[114] W. Feng, P. Ji, *Biotechnol. Adv.* **2011**, *29*, 889.
[115] G. Decher, *Science* **1997**, *277*, 1232.
[116] L. Deng, L. Shang, Y. Wang, T. Wang, H. Chen, S. Dong, *Electrochem. Commun.* **2008**, *10*, 1012.
[117] K. H. Hyun, S. W. Han, W. G. Koh, Y. Kwon, *J. Power Sources* **2015**, *286*, 197.
[118] M. Christwardana, K. J. Kim, Y. Kwon, *Sci. Rep.* **2016**, *6*, 30128.
[119] Y. Song, J. Cho, *Nanoscale* **2020**, *12*, 20141.
[120] Y. Ko, C. H. Kwon, S. W. Lee, J. Cho, *Adv. Mater.* **2020**, *32*, 2001924.
[121] Y. Ko, S. Lee, C. H. Kwon, S. W. Lee, J. Cho, *Adv. Energy Mater.* **2021**, *11*, 2002969.
[122] J. Ahn, W. Chang, Y. Song, Y. Son, Y. Ko, J. Cho, *Energy Storage Mater.* **2024**, *69*, 103396.
[123] E. Yong, D. Nam, Y. Kim, K. Kim, B. H. Kim, Y. Kim, J. Cho, *Energy Storage Mater.* **2023**, *60*, 102813.
[124] W. Chang, D. Nam, S. Lee, Y. Ko, C. H. Kwon, Y. Ko, J. Cho, *Adv. Sci.* **2022**, *9*, 2203800.
[125] Y. Song, S. Lee, Y. Ko, J. Huh, Y. Kim, B. Yeom, J. H. Moon, J. Cho, *Adv. Funct. Mater.* **2022**, *32*, 2106438.
[126] M. Kwon, D. Nam, S. Lee, Y. Kim, B. Yeom, *Adv. Energy Mater.* **2021**, *11*, 2101631.
[127] Y. Ko, M. Kwon, Y. Song, S. W. Lee, J. Cho, *Adv. Funct. Mater.* **2018**, *28*, 1804926.
[128] C. H. Kwon, Y. Ko, D. Shin, M. Kwon, J. Park, W. K. Bae, S. W. Lee, J. Cho, *Nat. Commun.* **2018**, *9*, 4479.
[129] T. Saha, R. D. Caño, K. Mahato, E. D. L. Paz, C. Chen, S. Ding, L. Yin, J. Wang, *Chem. Rev.* **2023**, *123*, 7854.
[130] C. H. Kwon, M. Kang, M. Kwon, D. Nam, Y. Song, E. Yong, M. Oh, Y. Kim, B. Yeom, J. H. Moon, S. W. Lee, J. Cho, *Appl. Phys. Rev.* **2022**, *9*, 021413.
[131] H. Sakai, T. Nakagawa, Y. Tokita, T. Hatazawa, T. Ikeda, S. Tsujimura, K. Kano, *Energy Environ. Sci.* **2009**, *2*, 133.
[132] P. Mishra, G. B. V. S. Lakshmi, S. Mishra, D. K. Avasthi, H. C. Swart, A. P. F. Turner, Y. K. Mishra, A. Tiwari, *Nano Energy* **2017**, *39*, 601.
[133] M. Sakthivel, S. Ramaraj, S. Chen, T. Chen, K. Ho, *ACS Appl. Mater. Interfaces* **2019**, *11*, 18483.
[134] Y. Yan, L. Guo, H. Geng, S. Bi, *Small* **2023**, *19*, 2301654.
[135] D. Maity, P. G. Ray, P. Buchmann, M. Mansouri, M. Fussenegger, *Adv. Mater.* **2023**, *35*, 2300890.
[136] P. Nithianandam, T. L. Liu, S. Chen, Y. Jia, Y. Dong, M. Saul, A. Tedeschi, W. Sun, J. Li, *Angew. Chem., Int. Ed.* **2023**, *62*, 202310245.
[137] J. Wang, N. He, J. Fei, Z. Ma, Z. Ji, Z. Chen, N. Nie, Y. Huang, *J. Power Sources* **2022**, *551*, 232190.
[138] J. Wang, M. Sun, X. Pei, L. Zheng, C. Ma, J. Liu, M. Cao, J. Bai, M. Zhou, *Adv. Funct. Mater.* **2022**, *32*, 2209697.
[139] T. Dey, I. Chauhan, S. Dutta, *ACS Appl. Electron. Mater.* **2023**, *6*, 4016.
[140] L. Wang, H. Shao, X. Lu, W. Wang, J. Zhang, R. Song, J. Zhu, *Chem. Sci.* **2018**, *9*, 8482.
[141] D. Lee, S. H. Jeong, S. Yun, S. Kim, J. Sung, J. Seo, S. Son, J. T. Kim, L. Susanti, Y. Jeong, S. Park, K. Seo, S. J. Kim, T. D. Chung, *Biosens. Bioelectron.* **2021**, *171*, 112746.

© 2024 The Author(s). Advanced Functional Materials published by Wiley-VCH GmbH

16163028, 2025, 16, Downloaded from https://advanced.onlinelibrary.wiley.com/doi/10.1002/adfm.202415933 by Korea University Library, Wiley Online Library on [20/09/2026]. See the Terms and Conditions (https://onlinelibrary.wiley.com/terms-and-conditions) on Wiley Online Library for rules of use; OA articles are governed by the applicable Creative Commons License

Junha Pak is an integrated M.S./Ph.D. candidate under Prof. Jinhan Cho at the Department of Chemical and Biological Engineering at Korea University. His current research is focused on developing novel biofuel cell electrodes and their energy conversion applications using a ligand replacement reaction-based layer-by-layer assembly.

Woojae Chang is a postdoctoral researcher at Korea University. He received his Ph.D degree in 2024 under the supervision of Prof. Jinhan Cho at the Department of Chemical and Biological Engineering at Korea University. His research is focused on the interfacial design of nanocomposite structures and their application to the development of novel textile-type energy storage electrodes.

Cheong Hoon Kwon has been a professor at the Department of Energy Resources and Chemical Engineering, Kangwon National University since 2022. She received her Ph.D. degree at the Department of Chemical and Biological Engineering at Korea University in 2008 and completed a postdoctoral fellowship at Harvard Medical School from 2009 to 2010. She then worked as a research professor at Hanyang University (2010–2016) and Korea University (2016–2022). Her research focuses on energy electrodes using metal nanoparticle-based interfacial assembly for biofuel cells, biosensors, energy harvesting, and electrochemical devices.

Jinhan Cho has been a professor at the Department of Chemical and Biological Engineering at Korea University since 2010. His research career started at POSTECH and Seoul National University, where completed his M.S. and Ph.D. degrees in 1997 and 2001, respectively. Then, he had post-doc courses at the Max Planck Institute of Colloids and Interface and the University of Melbourne. From 2003–2005, he was a senior researcher in LG Chemistry R&D Center. From 2006–2010, he worked as an assistant professor at Kookmin University. His research interests have been focused on studying the surface chemistry and electrochemical properties of various electrode materials.

© 2024 The Author(s). Advanced Functional Materials published by Wiley-VCH GmbH

16163028, 2025, 16, Downloaded from https://advanced.onlinelibrary.wiley.com/doi/10.1002/adfm.202415933 by Korea University Library, Wiley Online Library on [20/09/2026]. See the Terms and Conditions (https://onlinelibrary.wiley.com/terms-and-conditions) on Wiley Online Library for rules of use; OA articles are governed by the applicable Creative Commons License